Practical guide to the use of backgrounds in quantitative XPS

Cite as: J. Vac. Sci. Technol. A **39**, 011201 (2021); https://doi.org/10.1116/6.0000661
Submitted: 23 September 2020 . Accepted: 05 November 2020 . Published Online: 07 December 2020

Sven Tougaard

JVST A
Journal of Vacuum Science & Technology A

TUTORIAL

avs.scitation.org/journal/jva

Practical guide to the use of backgrounds in quantitative XPS

Cite as: J. Vac. Sci. Technol. A 39, 011201 (2021); doi: 10.1116/6.0000661
Submitted: 23 September 2020 · Accepted: 5 November 2020 ·
Published Online: 7 December 2020

Sven Tougaard[a)]

AFFILIATIONS

Department of Physics, Chemistry and Pharmacy, University of Southern Denmark, DK5230 Odense M, Denmark

Note: This paper is part of the Special Topic Collection on Reproducibility Challenges and Solutions.
[a)]**Electronic mail:** svt@sdu.dk

ABSTRACT

This guide is intended for both the novice in x-ray photoelectron spectroscopy (XPS) as well as users with some experience. XPS is one of the most widely used methods to characterize surface nanostructured samples, and XPS is now also commonly accessible to most material scientists through XPS facility centers. It is, therefore, increasingly used as a routine analysis technique to complement other techniques. This has led to an increase in the number of users who may not have a full understanding of the details of XPS and consequently must rely on the report provided by the XPS center. The purpose of this practical guide on the aspects of quantitative XPS is first to put the reader in a position to be able to understand and judge the meaning and possible errors in atomic concentrations based on analysis of peak intensities, which is the standard way quantitative XPS is reported. We discuss different ways to improve the analysis. This is attained by giving the reader a good understanding of how the intensities in the peak and the background of inelastically scattered electrons are linked together through the depth distribution of atoms. We then explore how this can be applied to greatly increase the capabilities of XPS to more accurately determine the composition and structure of surfaces on the nanoscale. This is possible at different levels of sophistication. We first see how a visual inspection of the XPS survey spectrum can be applied to get a quick rough indication of the structure. Next, we go through other more quantitative methods that are being used. The practical application of these techniques is illustrated by several examples.

I. INTRODUCTION

X-ray photoelectron spectroscopy (XPS)[1,2] is now the most widely used method to characterize surface nanostructures.[3] One of the reasons is that the distance λ traveled before an electron undergoes an inelastic scattering event is in the order of 1 nm[4] for electrons of energy between 100 and 1500 eV (which are typical for XPS). Therefore, the XPS peak intensity decreases strongly with the distance traveled in the solid and the information in the peak intensity comes from the outermost 5–10 nm of the sample.

XPS is applied to extract mainly two types of information: first, the exact energy of a photon excited core electron varies with the chemical state of the corresponding atom, and this is widely used to extract chemical state information of atoms in the surface region; second, the peak intensity provides information on the concentration of the corresponding atoms in the surface region, which is used to determine the atomic composition. Modeling of the background of inelastically scattered electrons is important for both types of analysis. However, here we are dealing with a third application of XPS where the background intensity of inelastically scattered electrons is used to enhance the extractable amount of information on the composition and structure of the surface region.

Most XPS instrument manufacturers provide software to facilitate quantitative analysis, and other software products are also available to support quantitative XPS analysis;[5–13] we will refer to some of these in this guide.

This paper is part of a series of practical guides on XPS.[14–19] The standard way to report quantification from XPS peak intensities is in the form of atomic percent based on a theory that assumes the sample composition is homogeneous. The samples we analyze with XPS are, however, typically inhomogeneous in the surface region, and it was pointed out many years ago[20,21] that this can result in huge errors in determined quantification based on peak intensities. Because of this, Shard[17] in his recent guide on XPS consequently recommends to use the phrase "equivalent homogeneous composition" when reporting quantification based on peak intensities.

In the present paper, we are concerned with this exact problem and we shall see how analysis of the distribution of inelastically scattered electrons in the background is applied to enhance the accuracy of quantitative XPS and also how the background is used to extract detailed information on the atom depth distribution in nanostructured samples.

The emphasis in this guide is to provide the XPS user, who is new to the topic with a good understanding of the interplay between peak and background intensities and further of how this can be applied to judge the accuracy of atomic concentrations determined from peak intensities and finally how it is applied for quantitative characterization of the composition and nanostructure of surfaces, ultimately with subnanometer depth resolution. For the experienced XPS user, much of the information given here will be well known and the presentation may seem a little lengthy. However, for the novice as well as the expert to be able to judge the accuracy of quantitative XPS in practical situations, it is necessary to have a full understanding of the processes involved. For the novice, I recommend to first read and get familiar with the implications and limitations of quantitative XPS as outlined in Secs. II, III, IV, V A and V E. This knowledge should be at the backbone of all XPS users, including those that do not acquire the data themselves but order the analysis from a central XPS facility. In Secs. V B–V D we discuss quantitative methods to apply the background to further increase the quantitative information from XPS. The final Sec. V E is at least as important as the remaining parts of this guide because there we emphasize that it is important to apply the background analysis wisely and ways to do this are described.

II. XPS BACKGROUND AND PEAK INTENSITY

The first aim of this guide on backgrounds in XPS is for the reader to understand the origin of the background and realize how the background and the peak intensity are linked together and how they both depend on the depth distribution of the photoemitting atoms. Such knowledge is required for the XPS user to be able to judge the uncertainty in and understand the meaning of the numbers that result from quantitative analysis based on peak intensities, which is the standard method used for XPS quantitation. The second aim of this guide is to make the reader aware of how this knowledge can be used to improve the accuracy of quantitative XPS analysis.

The spectra in Figs. 1 and 2 will be used in the different sections of this paper to illustrate the application of various methods to use the background for quantitative XPS. The spectra have been corrected for the analyzer transmission function, which varies with the kinetic energy E.[22] This correction is always important when XPS is applied for quantitative analysis. For many spectrometers, the transmission function varies approximately as E^{-m} with $m \sim 0.7$. Most commercial instruments will provide facilities to automatically do this correction.

Figure 1 shows AlKα excited XPS of a thin film of poly (styrene)-poly(dimethylsiloxane) (PS-PDMS) diblock copolymer[23] spin coated on a silicon wafer at room temperature and of the same sample after annealing at 130 °C for 20 h. The spectrum consists of peaks corresponding to the energy of core electrons, photon excited from Si, C, and O atoms. There is also a continuum intensity that

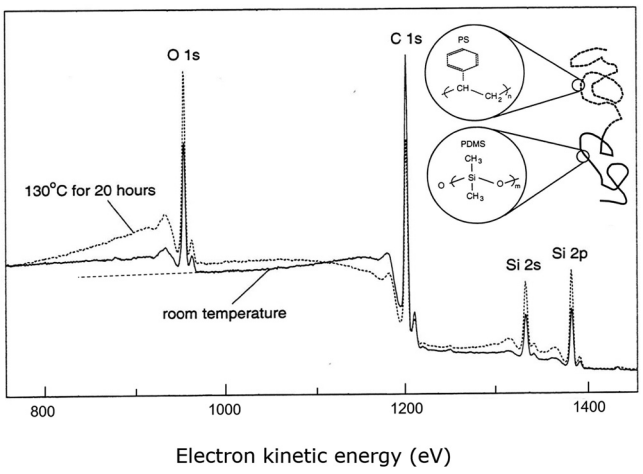

FIG. 1. XPS of a PS-PDMS diblock copolymer recorded at room temperature and after annealing at 130 °C for 20 h. Data from Andersen *et al.*, J. Electron Spectrosc. **121**, 93 (2001). Copyright 2001, Elsevier.

tends to increase at lower kinetic energies. These are photoelectrons that were originally excited at the peak energies, but have lost energy on their way to the surface. To analyze a single peak, the first step is to subtract the contribution to the background intensity from the peaks at higher kinetic (i.e., lower binding) energies. This is done by fitting a straight line to the intensity in an energy region

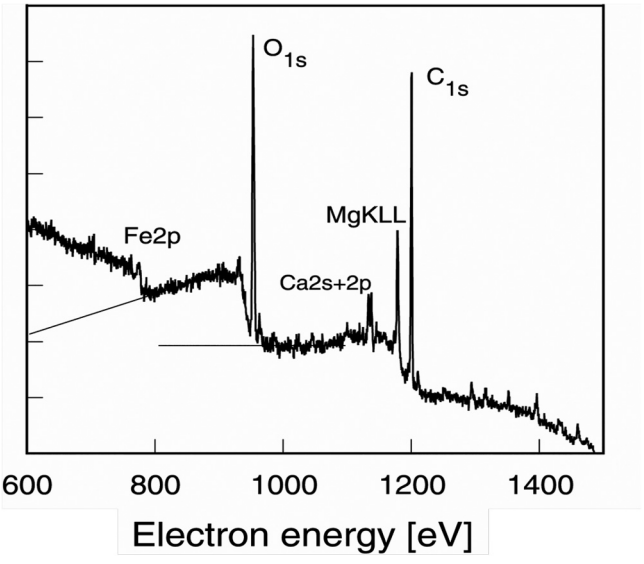

FIG. 2. Al Kα-excited XPS from an iron sample that had been exposed to a corrosive maritime environment. Reprinted with permission from Tougaard, *Software Packages to Characterize Surface Nano-Structures by Analysis of Electron Spectra* (www.quases.com, 2020). Copyright 2020, www.quases.com.

on the high kinetic energy side of the peak as illustrated for the O1s peak by the dashed line in Fig. 1. After subtraction of the intensity below this line from the spectrum, the contribution from the O1s peak to the spectrum has been isolated. In this paper, we will denote this spectrum as J(E).

Figure 2 shows an AlKα excited XPS spectrum of an iron sample that had been exposed to a corrosive maritime environment.[24] The intensity and shape of the peak and background below the O 1s and the Fe 2p peaks are very different, which is due to different depth distributions of oxygen and iron atoms. As we shall see, the quantification accuracy can be greatly enhanced when the background is included in the analysis.

To be able to use the peak intensity for quantification, the background must first be subtracted from the spectrum. The data analysis software that comes with most instruments will typically have at least three ways to do this:[16,17,19] (1) a straight line drawn from above the peak to a point below the peak, (2) the "Shirley background,"[25] which is also used between two energies below and above the peak by an algorithm that assumes the background intensity at a given energy to be proportional to the total intensity at higher energies, and (3) an algorithm,[26] which is based on a physical model for the inelastic scattering properties of the material; this latter method has become known as the "Tougaard background".

For a linear background, a straight line is drawn from a point close to the low energy side of a peak, E_{min}, to a point on its high energy side, E_{max}, and subtracted from the peak. One of the problems with this method is that it is not well defined since the choice of low and high energy points is entirely subjective.[27] The Shirley background[25] subtraction is an iterative procedure, based on the algorithm

$$F^{n}(E) = J(E) - k_n \int_{E}^{E_{max}} F^{n-1}(E') \cdot dE, \quad (1)$$

where $F^0(E) = J(E)$ and k_n is found from the requirement that $F^n(E_{min}) = 0$. The series converges rapidly and after three to four iterations, $F^n(E) \sim F^{n-1}(E)$. The values E_{min} and E_{max} have to be chosen by the operator. The method is rather independent of E_{max}, but does depend on E_{min}, so the Shirley background is thus also not well defined. When it is applied over a small energy range, the peak areas derived are similar to those found using the straight line method. To minimize the uncertainty, it is important to be consistent in picking E_{min} and E_{max} by using the same criteria (although also entirely subjective and based on visual observation) for all peaks.[27]

The Tougaard background[26] relies on a quantitative description of the physical processes that lead to the background. It comes in various forms depending on the situation[10,21] and the simplest algorithm is

$$F(E) = J(E) - B_1 \int_{E}^{E_{max}} J(E) \frac{E' - E}{(C + (E' - E)^2)^2} \cdot dE', \quad (2)$$

where $C = 1643\ eV^2$. The factor B_1 is adjusted to give zero intensity in a region between 30 and 50 eV below the characteristic peak structure. For polymers, and other materials (such as Si and Al) with a sharp plasmon structure, the three-parameter Tougaard-background algorithm is more accurate,[28]

$$F(E) = J(E) - B_1 \int_{E}^{E_{max}} J(E') \frac{E' - E}{(C - (E' - E)^2)^2 + D(E' - E)^2} \cdot dE', \quad (3)$$

where C and D depend on the material. The kernel in the integrals reflect the cross section for inelastic scattering in the material, and for complex systems, where the photoelectron may pass layers of material with widely different scattering properties, a mixture of the corresponding cross sections gives a more accurate description of the background.[29,30] Figure 3 shows the full AlKα excited spectrum from a Cu foil analyzed by Eq. (2).[26] As can be seen, the inelastically scattered electron background is described with good accuracy over the full 1000 eV energy range. Note also that the peaks extend to ~30 eV on the low energy side of the characteristic peaks. The intensity in this energy range arises from the intrinsic (or shake-up) electrons.[31] As was described above, when this method is applied to a single peak, a straight line is first fitted to the spectrum on the high energy side of the peak, and then subtracted from a region of the spectrum whereby the peak and background intensity originating from a given core level is isolated. Such straight line backgrounds are shown in Figs. 1 and 2.

Figure 4 shows the Si2p,2s spectra from SiO_2 (Ref. 24) analyzed by Eq. (2) (with $C = 1643\ eV^2$) (upper) and by Eq. (3) [using $C = 542$ and $D = 275\ eV^2$, valid for SiO_2 (Ref. 28)] (lower). SiO_2 has

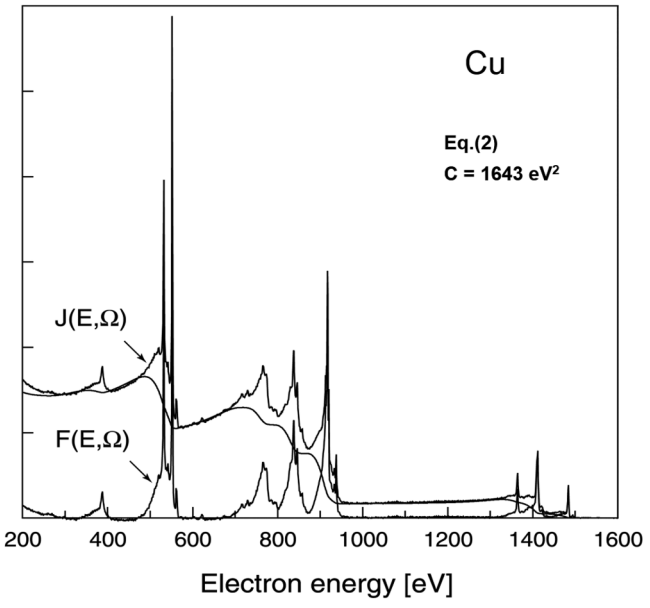

FIG. 3. Al Kα-excited spectrum J(E) of pure copper, and the primary excitation spectrum F(E) determined from Eq. (2) with C = 1643 and B1 = 3010 eV². Reprinted with permission from Tougaard, Surf. Sci. **216**, 343 (1989). Copyright 1989, Elsevier.

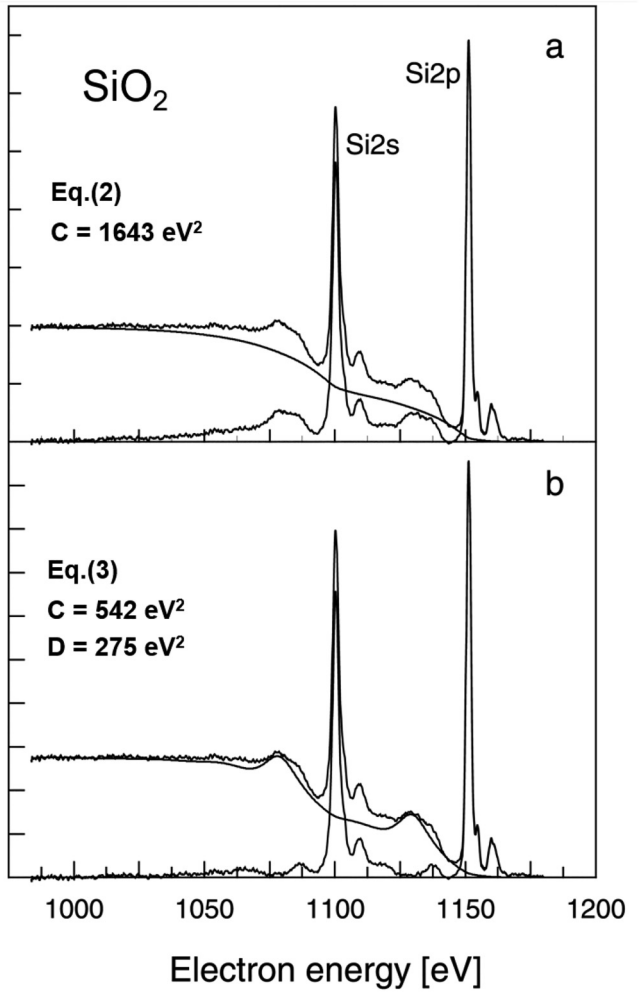

FIG. 4. Mg Kα-excited XPS of pure SiO_2 and the background-corrected spectrum using Eq. (2) with C = 1643 and B1 = 3510 eV^2 and Eq. (3) with C = 542, D = 275, and B1 = 306 eV^2.

a narrow plasmon at ~23 eV, and while Eqs. (2) and (3) both give consistent and good background correction beyond ~40 eV from the Si 2s peak, Eq. (3) accounts better for the intensity in the plasmon energy loss structure. This illustrates that while Eq. (2) has been shown to be good for many transition metals, their alloys, and oxides, Eq. (3) is better when the material has sharp plasmon loss features.

Since Eq. (2) accounts so well for the background in Fig. 3 it is obvious that it gives a quite accurate description of the inelastic scattering processes that are responsible for the background. Equation (2) does, however, only apply for homogeneous and exponential atom depth distributions.[32] For other depth distributions, different and more complex algorithms apply[10,32–34] as discussed in Secs. V C and V D. Although the Shirley and straight line methods are not based on physical models and have been found to be less accurate,[27,35] they still give a reasonably accurate *relative* measure for the peak area. The two methods have the advantage that only the main peak region (typically of width less than 5 eV) needs to be analyzed, while proper use of the Tougaard background requires a wider energy range. In practice, the Shirley and straight line backgrounds are widely used.[16,17,19]

It is straightforward to model the measured intensity of a peak, which has contributions from photoelectrons excited at atoms over a range of depths. It drops exponentially with the path traveled (see Fig. 5), and the contribution dI_A to the measured peak intensity, which originates from photon excited electrons with intensity I_0 at depth z at an angle θ to the surface normal, is attenuated with the distance $z/\cos\theta$ the electron travels before reaching the sample surface and

$$dI_A = I_0 \cdot X_A(z) \cdot e^{-\frac{z}{\lambda\cos\theta}} dz. \tag{4}$$

Here $X_A(z)$ is the atomic concentration of atoms A in a thin layer dz at depth z. We have here assumed that the electrons move along straight lines as in Fig. 6(a). Angular deflection due to elastic scattering as in Fig. 6(b) will also occur, and the implication of this is examined in Sec. II A.

The measured peak intensity (or peak area) I_A has contributions from atoms at all depths and from Eq. (4),

$$I_A = \int_0^\infty I_0 \cdot X_A(z) \cdot e^{-\frac{z}{\lambda\cos\theta}} dz. \tag{5}$$

Since λ is ~0.5–3 nm,[4] the exponential factor drops quickly with depth z and is negligible for $z > 3\lambda$.

The left-hand panel of Fig. 7 shows model spectra (generated with the QUASES software[11]) from Au atoms in a 1 nm thick layer situated at different depths in a Cu sample with $\lambda = 1.5$ nm. The same amount of Au atoms gives a hugely varying intensity because electrons excited at larger depths have a smaller probability [by Eq. (4)] to survive at the peak energy but (see Fig. 5) are likely to lose energy and end up at lower energies in the spectrum. This is clearly seen as an increase in the background intensity below the peak energy and a corresponding decrease in the Au4d peak intensity as the 1 nm thick gold layer is buried at increasingly larger depths.

The intensity of both the peak and the background varies substantially and in opposite directions with depth: the peak intensity decreases and the background intensity increases as the layer is placed at larger depth. The ratio of the two gives, therefore, a very sensitive parameter, which can be applied to estimate the depth or thickness of the layer as was suggested and explored many years ago[36] (see Sec. V B below).

A. Correction for elastic electron scattering effects

It is well known that angular deflection will occur,[6,7,37–43] and this can affect the measured peak intensity. However, in many practical cases, the effect turns out to be small. Thus, in a study of peaks from seven pure metals,[44] the theoretical peak intensities were found to change by an average of 14% as a result of elastic scattering but the standard deviation from experiment was practically the same, namely, ~15% independent of whether or not elastic scattering is included. This implies that the contributions

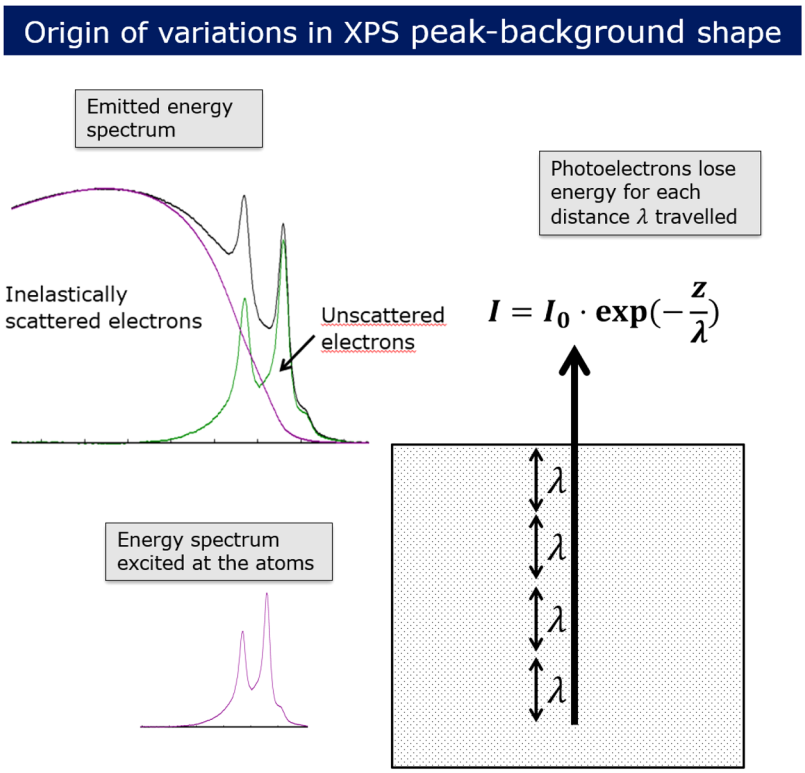

FIG. 5. Interplay between XPS peak intensity, inelastic background, and depth of origin.

from errors in other parameters, such as the photoionization cross sections and the inelastic electron mean free path, are so large that they overshadow the improvements by including elastic electron scattering in analysis of homogeneous solids.[44] In agreement with this result, it was found both experimentally[38] and theoretically[39,41] that the effect of elastic scattering is small (although not negligible) for small depths z but can be substantial for large θ and for $z > 2\lambda$. We will now discuss how these results can be used in practical analysis.

In Eqs. (4) and (5), it was assumed that the photoelectron moves along a straight line on its way to the spectrometer as shown in Fig. 6(a). However, the electron can also start out in a different direction and later be deflected by elastic electron scattering into the direction of the spectrometer as illustrated by trajectories (b),

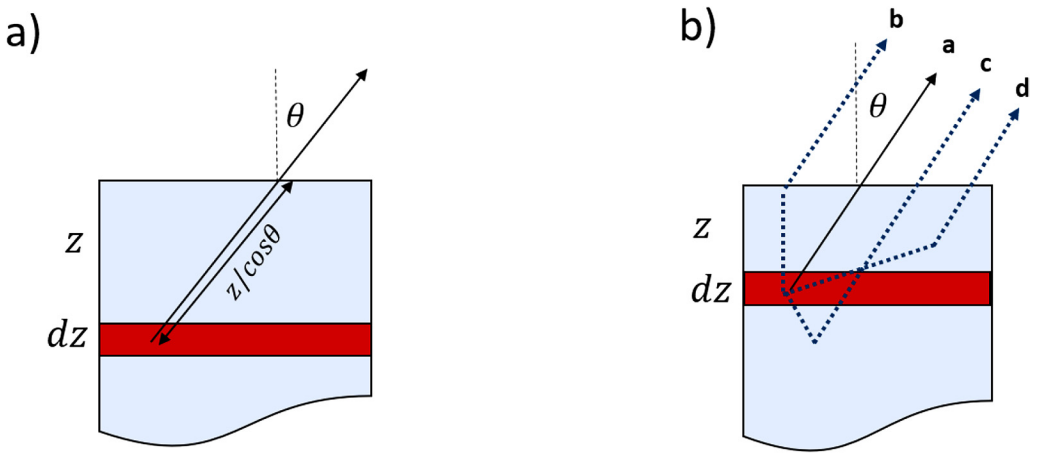

FIG. 6. Possible electron trajectories when elastic deflection is (a) ignored and (b) included.

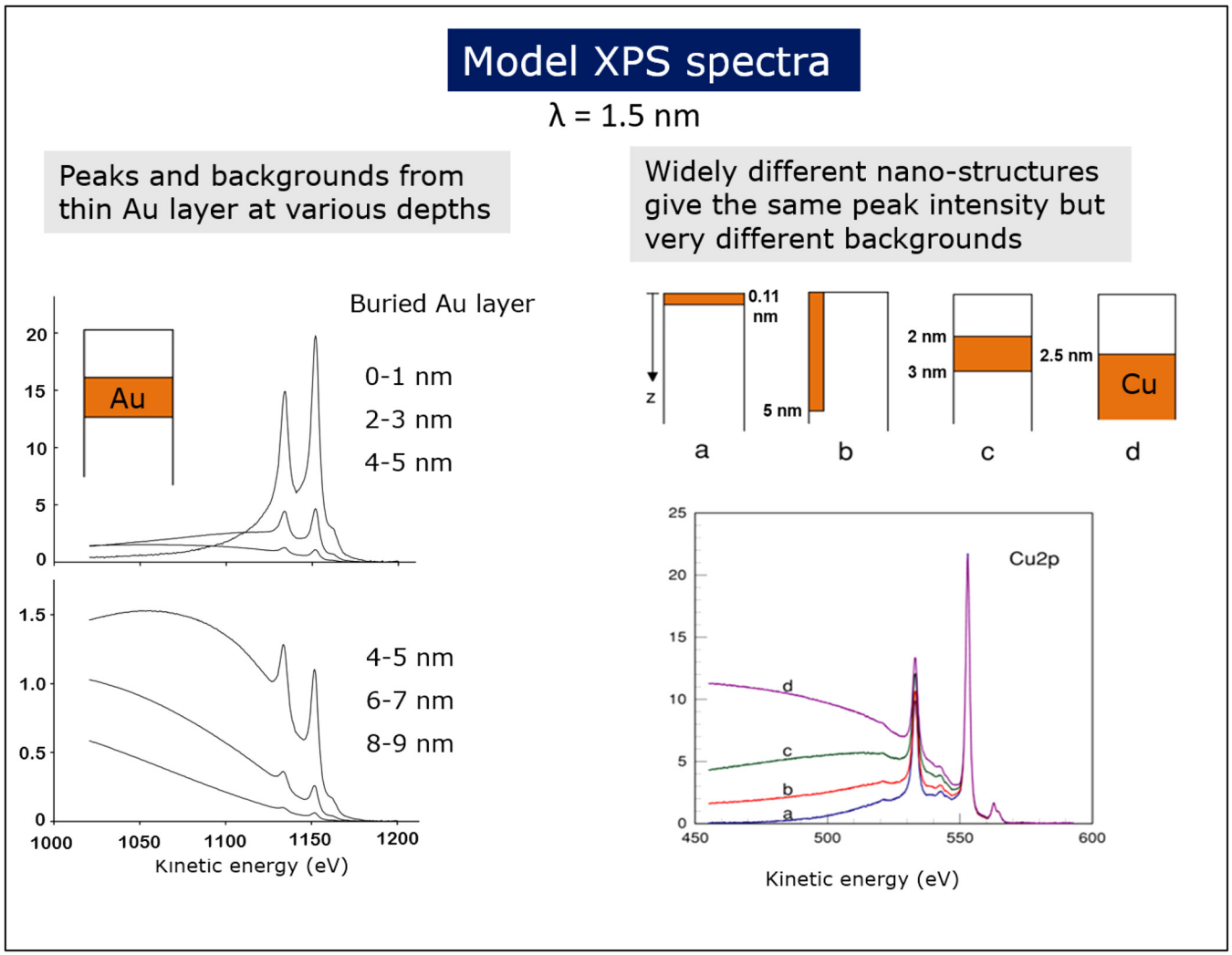

FIG. 7. Left panel: Au4d spectra from a 1-nm-thick Au layer at different depths in a material with λ = 1.5 nm calculated with the QUASES software (Ref. 11). Right panel: Cu2p spectra from Cu atoms with different concentration distributions in an Au matrix. Adapted with permission from Tougaard, J. Vac. Sci. Technol. A **14**, 1415 (1996). Copyright 1996, American Vacuum Society.

(c), and (d) in Fig. 6(b). The intensity from electron (b) will be attenuated less than electron (a) because it has traveled a shorter distance in the sample. In contrast, electrons (c) and (d) have traveled a larger distance in the material than electron (a) and consequently their intensity will be attenuated more. So the intensity from some electrons is attenuated less while other electrons are attenuated more than electron (a). This canceling effect tends to reduce the effect of elastic scattering, especially for shallow layers.[38]

Tougaard and Jablonski[39] suggested to describe this deflection effect on the peak intensity by a simple correction factor (CF) to Eqs. (4) and (5),

$$dI_A = I_0 \cdot CF(z) \cdot X_A(z) \cdot e^{-\frac{z}{\lambda \cos\theta}} dz, \tag{4a}$$

$$I_A = \int_0^\infty I_0 \cdot CF(z) \cdot X_A(z) \cdot e^{-\frac{z}{\lambda \cos\theta}} dz. \tag{5a}$$

To obtain general knowledge on CF, they first determined CF by performing extensive Monte Carlo calculations made under variations in the full relevant range of electron energy, matrix atoms, depth of origin of emitted electrons and angular emission anisotropy.[39]

They then discovered that although CF was found to depend strongly on all these parameters, the main variation can be described by a single parameter, which is a reduced depth expressed as z/λ. This is shown in Fig. 8(a). Note that for each depth, 60 values are shown, corresponding to the five

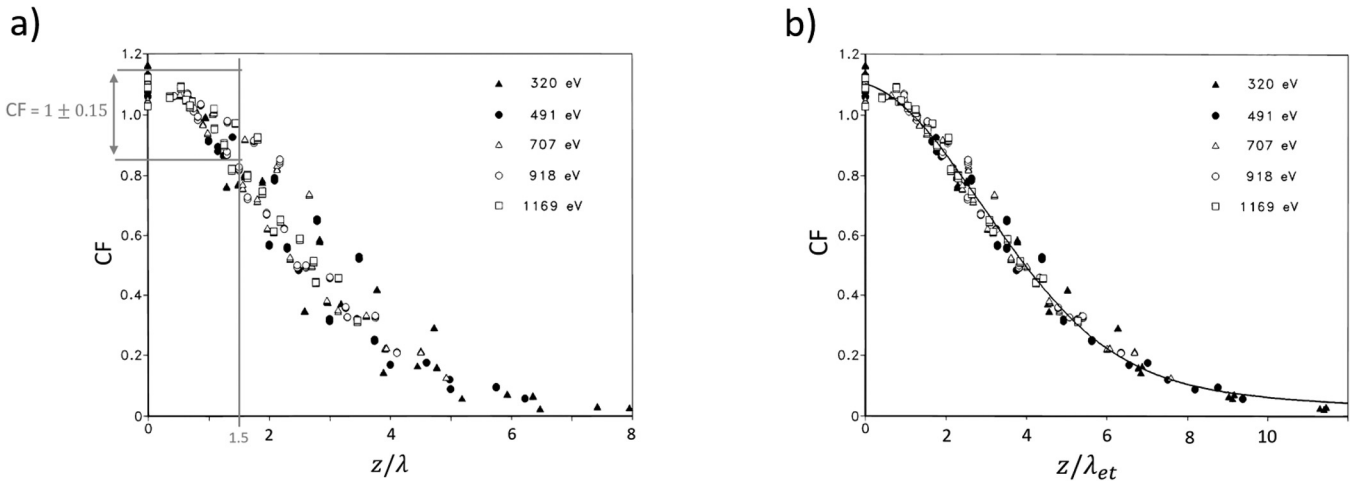

FIG. 8. Elastic electron scattering CF in Eqs. (4a) and (5a) plotted as a function of the reduced lengths z/λ and z/λ_{et}, respectively. Reprinted with permission from Figs. 4 and 5 in Jablonski and Tougaard, Surf. Interface Anal. **26**, 17 (1998). Copyright 1998, John Wiley & Sons, Ltd.

photoelectron energies, four different matrix atoms, and three asymmetry parameters.[39] This general variation with z/λ can be used to get a rough estimate of the effect. As seen from Fig. 8(a), the effect is small and less than ~15% for depths $z < 1.5\lambda$ due to the above-mentioned cancellation effect and in agreement with experiments.[38,44] However, it can be substantial for larger depths and CF ~ 0.5 for depth ~3λ. For a thin layer at the surface, CF is seen to be about 5%–10% larger than 1, which is due to electrons being backscattered from the substrate, like electron (c) in Fig. 6(b), resulting in a larger intensity compared to the situation where the substrate is not present. The general dependence of CF in Fig. 8(a) can for $\frac{z}{\lambda} < 4$ be approximated by

$$CF\left(\frac{z}{\lambda}\right) = 1.27 \cdot \exp\left(-0.1\left(\frac{z}{\lambda}\right)^2 - 0.14\right). \quad (6)$$

The scatter in Fig. 8(a) is, however, still considerable, and they then found[39] that the variation of CF is even better described by the reduced depth z/λ_{et} where

$$\lambda_{et} = \frac{\lambda \cdot \lambda_{tr}}{\lambda + \lambda_{tr}}, \quad (7)$$

and λ_{tr} is the transport mean free path. This is seen in Fig. 8(b), where the best fit to the data is given by the formula[39]

$$CF\left(\frac{z}{\lambda_{et}}\right) = \exp\left(-0.157\,764 \cdot \left(\frac{z}{\lambda_{et}}\right) - 1.251\,32\right) + \exp\left(-0.056\,241\,7 \cdot \left(\frac{z}{\lambda_{et}}\right)^2 + 0.006\,988\,49 \cdot \left(\frac{z}{\lambda_{et}}\right) - 0.201\,962\right). \quad (8)$$

Jablonski and Tougaard also studied the variation of CF with the geometry of the experimental setup and found[41] that Eq. (8) is of general validity provided that the angle of emission is <30° with respect to the surface normal and the angle between x-ray anode and analyzer axis is 45°–65°, which are typical for most experimental setups. Outside of this range, a more involved formula[40] is more accurate. Facilities to calculate CF according to Eqs. (6) and (8) are available in the free QUASES-IMFP-TPP2M software.[13] The approximate correction given by Eq. (8) was applied in Refs. 38, 45, and 46.

Determined peak intensities by analysis with Eq. (4) should be divided by CF to obtain the peak intensity corrected for elastic scattering.

Finally, we mention that elastic electron scattering can also affect the shape of the background.[47,48]

III. QUANTIFICATION AND THE ATTENUATION FACTOR PROBLEM

Quantitative XPS is usually based on measured peak areas calculated after the background has been subtracted. This approach is widely used but it is important to understand and be aware of the inherent errors that can be associated with this as was pointed out many years ago.[20,21] We will now briefly discuss this problem.

In traditional quantitative XPS analysis,[1,2,16,17,21] it is assumed that the sample is homogeneous so the concentration of atoms X_A

is constant in the outermost ~5–10 nm of the sample and integration of Eq. (5) gives

$$I_A = I_0 \cdot X_A \cdot \lambda \cdot \cos\theta. \tag{9}$$

So, the peak area is proportional to the atomic concentration. I_0 depends on various factors that are determined either by using reference spectra or they are taken from tables with, e.g., photoionization cross sections. Finally, one obtains from Eq. (9) (Refs. 1 and 49),

$$X_A = F \cdot I_A, \tag{10}$$

where F is a factor which includes the effects of the elastic and inelastic mean free paths, the photoionization cross section, characteristics of the spectrometer, and renormalization corresponding to the intensity from the other elements in the sample. Within this model, the surface concentration X_A is proportional to the measured peak intensity or peak area I_A.

For accurate analysis, it is important to have good values for F and to use an accurate background subtraction method to determine I_A. However, the by far most serious problem with the use of Eq. (10) for practical XPS analysis is not related to the accuracy of F or I_A but to the assumption of surface homogeneity in the outermost ~3λ (or ~5 nm) of the sample[21] (see Fig. 9).

As noted in Ref. 21, the problem with Eq. (10) is that it is only valid when the concentration is constant in the surface region. In practice, it is however quite rare that the samples we analyze with XPS are homogeneous in the outermost few nanometers. In fact, the reason why we use XPS, rather than bulk sensitive techniques, is that the sample composition is inhomogeneous on the nanometer depth scale. So, for real practical samples, the concentration varies often significantly in the topmost 0–5 nm and Eq. (10) is invalid for quantitative analysis of such samples.

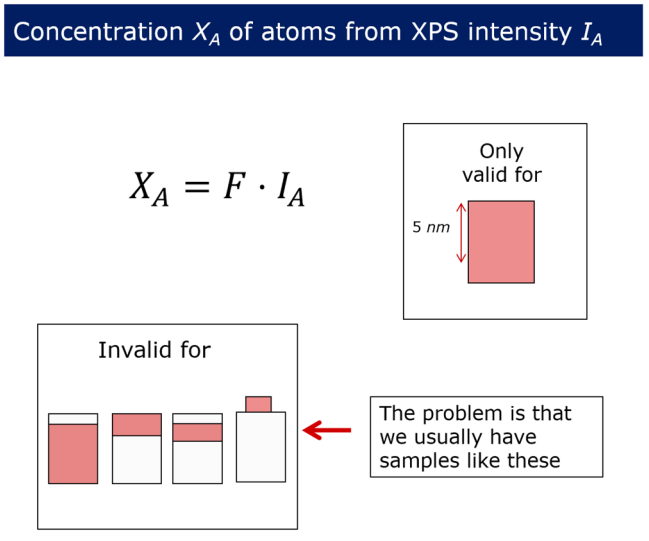

FIG. 9. Procedure for XPS analysis that is used in most labs. F is defined in the text. This illustrates the limitations of this formalism for practical surface analysis since it is not valid for many samples of practical interest. Reprinted with permission from Fig. 1 in Tougaard, Surf. Interface Anal. **50,** 657 (2018). Copyright 2018, John Wiley & Sons, Ltd.

The origin of the problem is illustrated in the right-hand panel of Fig. 7 (Ref. 21) that shows model spectra with identical Cu2p photoelectron peak intensities that are obtained from four Cu/Au samples with very different morphologies. This arises because the peak intensity is attenuated with depth as in Eq. (4). So, the observed Cu2p peak intensity can either come from a 0.11 nm thick Cu layer on an Au substrate, from a 5 nm thick $AuCu_4$ alloy, from a 1 nm thick layer at 2–3 nm depth, or from a Cu substrate covered with a 2.5 nm thick Au overlayer. So, the peak intensity alone carries only limited quantitative information on the composition of the sample in the surface region.

As a practical example that illustrates the problems with this formalism, Fig. 10 shows the spectrum from a sample that consists of Au and Ni atoms. Traditional analysis with Eq. (10) (performed with the CASAXPS software[8]) gives the composition table shown in the inset of the upper left part of Fig. 10 (there is a small C contamination that has been ignored). The conclusion is that the surface region consists of an alloy with composition $Au_{0.84}Ni_{0.16}$. But as illustrated in the top part of Fig. 10, the same ratio of Au4d to Ni2p peak intensities could originate from other structures where the surface concentration of Au can be anywhere from 0% to 100%. (The lower part of Fig. 10 is discussed in Sec. V A.) The problem is that the attenuation of the peak intensity depends strongly on the depth distribution of the atoms, which is ignored in Eq. (10).

IV. METHODS TO CORRECT FOR THE PEAK ATTENUATION FACTOR

The peak attenuation factor is here defined as the factor that accounts for the attenuation of peak intensity corresponding to the actual depth composition of the analyzed sample rather than as in Eq. (10) where the distribution in the surface region has been assumed to be constant. From the above, it is obvious that a meaningful quantification cannot be made without taking this attenuation factor into account.

As was discussed in a recent paper,[49] there are essentially three methods to make this correction. We will focus here on the use of the background to correct for the attenuation factor. However, to put this into perspective, we will first briefly mention two other methods that are frequently applied.

A. From assumed knowledge of sample morphology

If the morphology of the sample is known, it is a very simple calculation to correct for the attenuation factor.[1,2,50] The mathematics will be different depending on the type of morphology (thin layer, buried layer, islands, exponential diffusion profile, etc.) and is shown for a thin film in Fig. 11, but the calculation is straightforward for all types of morphologies. The problem is that this analysis procedure is only possible if one knows the morphology of the sample before the analysis is done. However, it is very rare that we know the structure. It is exactly because we do not know the structure of the sample that we do XPS analysis. Sometimes we may

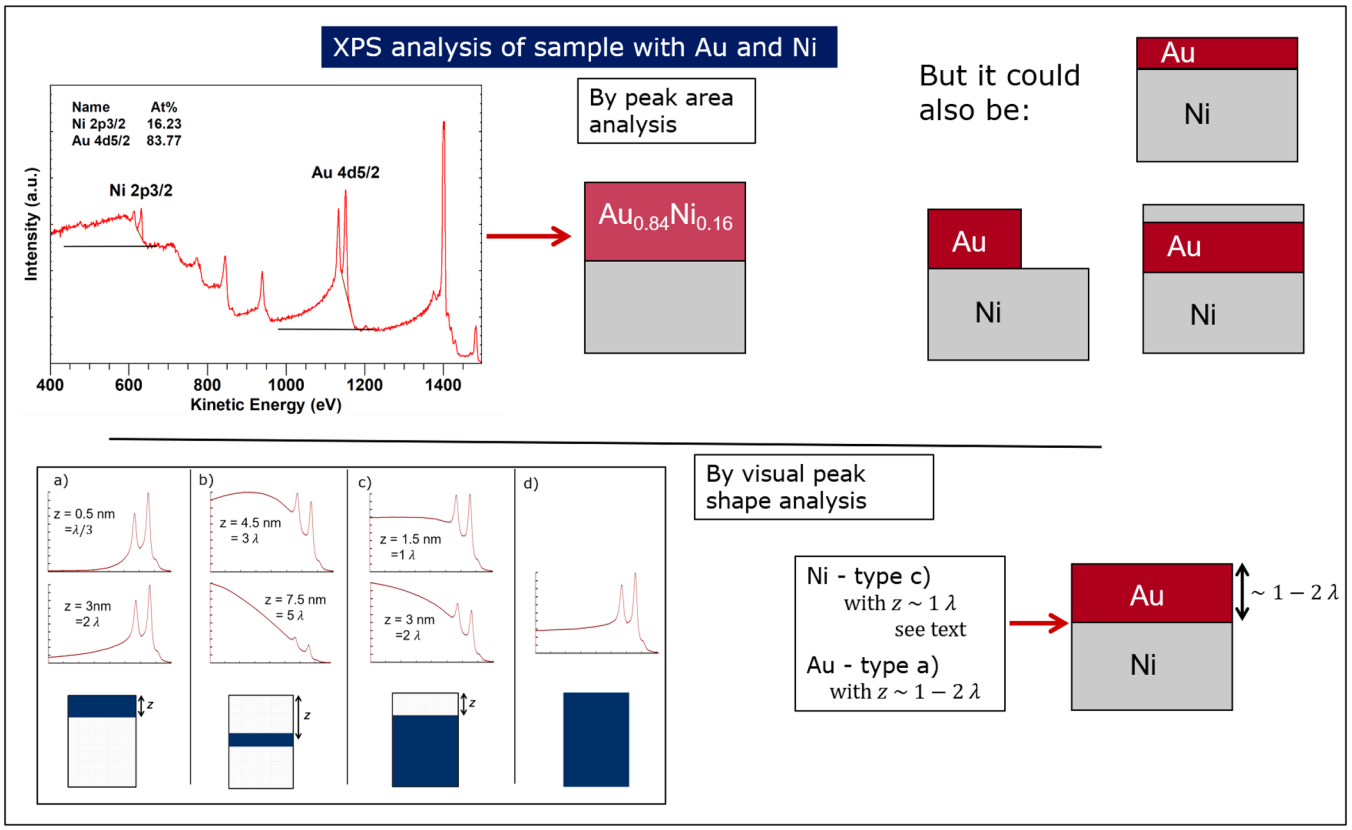

FIG. 10. XPS analysis of a sample based on peak areas. The upper right part illustrates that because of the peak attenuation effect, it is not possible to distinguish between different possible structures. The lower part shows model Au4d XPS for different distributions of Au atoms, in a host material with $\lambda = 1.5$ nm. The lower right part shows how these can be used to determine the rough structure of the sample using visual peak shape analysis. Adapted with permission from Tougaard, Surf. Interface Anal. **50,** 657 (2018). Copyright 2018, John Wiley & Sons, Ltd.

think we know the structure, if, e.g., A atoms are deposited on a substrate consisting of B atoms. But it is very unlikely that growth continues in a layer by layer fashion and typically it proceeds with the formation of islands, and we may also have diffusion or chemical reactions between the atoms. Therefore, one should be cautious when using this approach to correct for the attenuation factor unless the structure of the sample has been determined by another technique.

B. From angle resolved XPS

A second approach that is often applied to take the peak attenuation effect into account is angle resolved XPS (ARXPS) where the spectrum is measured at a range of emission angles.[51–53] Due to the variation in path lengths with the angle, a difference in the measured peak intensity [given by Eq. (4)] is seen and this is compared with model calculations. This method works very well for flat surfaces and is used extensively in the semiconductor industry.[54] The main limitation is that it does not work for rough surfaces, and it also fails even for nanostructures grown on an otherwise very flat surface.[55] This is because the structure on the surface will cause the photoelectrons to pass an undefined length in the material for large emission angles. This can be minimized if large angles are not included in the ARXPS analysis. However, the change in the path length with angle θ is proportional to $1/\cos(\theta)$ [Fig. 6(a)], which does not vary much for small angles [e.g., $\cos(30^\circ) = 0.87$] so the change in path length is 13%, which gives only a small variation in the intensity [Eq. (4)] and larger angles are needed to get significant depth information from ARXPS.[51] When large angles of emission (>60°) are included, elastic scattering effects become substantial[41] and it is important that the analysis includes the influence of elastic electron scattering. The analysis is done with software and some general XPS software systems will provide facilities to do the analysis. A software exclusively for ARXPS is also available.[12]

C. From analysis of the XPS background

The third method to correct for the attenuation effect is based on analysis of the spectrum in a wide energy range, which includes both the peak and the background.[10,11,32,56,57] This method relies

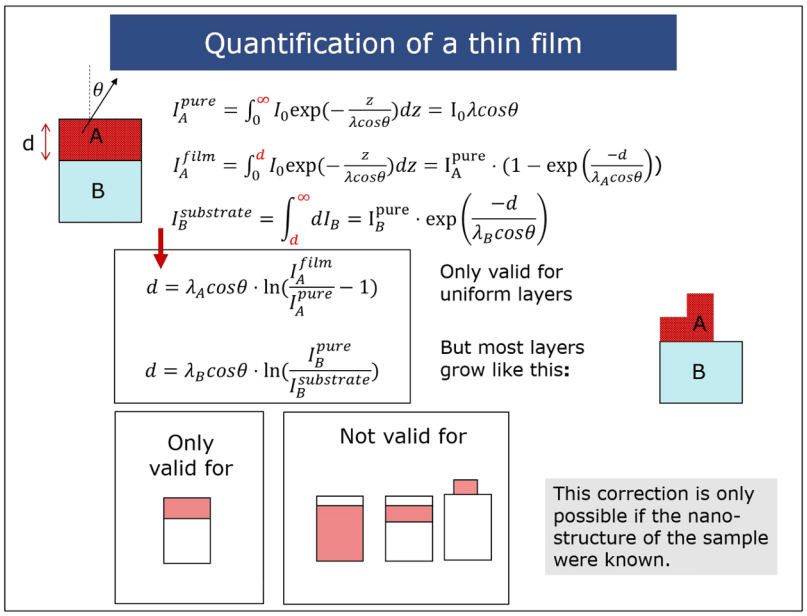

FIG. 11. This figure illustrates that it is easy to correct for the peak attenuation effect if the structure of the sample is known. In most practical cases, this is however not possible because the structure is not known. So, this correction procedure is in general not possible. Reprinted with permission from Fig. 4 in Tougaard, Surf. Interface Anal. **50**, 657 (2018). Copyright 2018, John Wiley & Sons, Ltd.

on the fact that the spectrum varies substantially with the sample structure (Fig. 7) and is discussed in Sec. V. It does not have the limitations of the other two: first, no *a priori* information on the structure of the sample is needed because this is found from the peak-background shape, and second it also works for rough and nanostructured surfaces because all information is deduced from a single spectrum, which, when taken close to the surface normal, does not have the structure limitation inherent of ARXPS. The main limitation of this technique is that although in principle it is easy to apply, its application can become complex if there is a peak from another element nearby the peak being analyzed (see Sec. V E).

V. USE OF THE BACKGROUND AT DIFFERENT LEVELS OF SOPHISTICATION

The characteristic changes in the peak shape and intensity over a wide energy range (which we here refer to as the peak-background shape) seen in Figs. 1, 2, and 7 can be applied to tremendously enhance the accuracy of quantitative XPS analysis. This is so because the effect is huge, and the intensity, say 30 eV below the peak energy in Fig. 7, varies by orders of magnitude for different structures. While it is not possible to distinguish between the structures in the right-hand panel of Fig. 7 from the peak intensity alone, they are easily distinguished by the intensity in the background. This is the philosophy behind XPS characterization with the QUASES software,[10,11] which has become increasingly used in routine XPS analysis in recent years and in Sec. V D a brief introduction to this software is given. However, simpler methods can also give valuable, although less quantitative, information on the sample structure and composition. In subsections V A–V E, we will discuss several approaches that have been developed since the early 1980s. They rely on an analysis of the inelastic background in a ~100 eV energy loss range below the peak.

However, before moving on, we mention here a recent interesting approach by Shard and Spencer,[58] using the part of the background where the photoelectron has lost several hundreds of electron volts of energy to measure thick organic films. When the organic film is deposited on, e.g., a gold substrate, the background from the substrate peaks was found to vary with film thickness in a characteristic way over the full ~1000 eV energy range of the spectrum. Studying spectra from a range of organic layer thicknesses, they found a semiempirical procedure, which can be applied to get information on both the thickness and the uniformity of organic films.[58]

A. Visual inspection of the survey spectrum

The simplest way to get information on the nanostructure of a sample is by a visual inspection of the survey spectrum. This possibility was systematically explored in a recent paper[49] where standard model spectra were calculated for various nanostructured samples, and these are used for a visual determination of the approximate sample structure. The spectra in Fig. 7 are examples of such spectra and further model spectra from different depth distributions are shown in the lower part of Fig. 10. When comparing these peak-background shapes to the spectrum of the AuNi sample in the upper part of Fig. 10, it is clear that Au is surface localized while Ni is in the bulk. Then, it is immediately concluded that the sample structure consists of bulk Ni with a thin layer of Au on top. This is consistent with the fact that the sample was produced by evaporating Au on an Ni substrate. This gives more useful information compared to the atomic concentrations determined from peak areas. The determined structure is in rough agreement with a more accurate quantification with QUASES software,[59] which showed that

TABLE I. Results from analysis of the spectrum in Fig. 10.

Method of analysis	Au	Ni
Visual inspection (Sec. V A)	Surface layer	Subsurface
A_p/B (Sec. V B)	46 eV	9.2 eV
QUASES (Sec. V D)	3 nm tall islands covering 68% of the surface	—

Au forms 3 nm tall islands that cover 68% of the surface. In Ref. 59, the results are also compared to Rutherford backscattering (RBS) analysis of the same sample, and they were found to agree to within 7% (only the amount of Au, not the formation of islands can be determined by RBS). (The results are summarized in Table I.) The application of this simple visual technique was demonstrated for several other practical cases in Ref. 49. The reader is encouraged to study these examples to become acquainted with this visual method.

Application of the method to visually analyze the spectrum in Fig. 1 is a little more involved than the examples in Ref. 49 but illustrates further capabilities of the method: The first impression from the spectra in Fig. 1 is that at room temperature the peak-background shape of both O1s, C1s, and Si2p,2s resemble the spectrum in Fig. 10(d), indicating that the sample composition is roughly homogeneous and the distribution of the PDMS-PS is, therefore, also roughly homogeneous. After annealing, the O1s and Si2s,2p peak intensity is seen to increase. This immediately tells us that there is a redistribution of O and Si atoms to become more surface localized and since O and Si are only in PDMS and not in PS, this implies that the PDMS end of the diblock copolymer has segregated to the surface. Further inspection shows that upon annealing, not only the O1s and Si2p,2s peak intensities have increased but the inelastic background has increased over a wide energy range. This shows that the oxygen and silicon concentrations have increased not only at the immediate surface but over a larger range of depths. Since the intensity increase extends over ~100 eV energy loss, it must have increased over depths of several λ. In a similar (but opposite) way, not only the C1s peak intensity decreases but also the inelastic background decreases over a wide energy range below the C1s energy. This implies a decrease in carbon concentration in the near surface region over depths of several λ. At the same time, the background intensity far below all peaks remains approximately unchanged after annealing. Since the electrons observed at energies far below the peaks originate from atoms at deep layers, this shows that the composition at deeper layers (>5–10λ) is roughly unchanged.

So, putting these pieces of information together: Upon annealing, the PDMS end of the diblock copolymer has segregated to the surface over depths of several λ, but the bulk distribution at deeper layers is roughly unchanged. This is consistent with the behavior of the C1s peak-background region since the C concentration is smaller in PDMS compared to PS. This structure is in good agreement with the QUASES analysis in Sec. V D (see Fig. 18 below), which shows that PDMS segregates to the surface in a ~14 nm thick layer.

Quantitative account for these observations is confirmed by the model spectra in Fig. 12, which show spectra of an $Au_{0.8}Cu_{0.2}$ alloy before and after surface segregation of Au in a layer of thickness 0.5λ and 2.0λ, respectively. Segregation in a 0.75 nm thin layer is seen to cause the peak intensity to increase while the background is largely unchanged; segregation in a 3 nm thick layer results in an intensity increase of not only the peak but also of the inelastic background over a range that extends to ~100 eV below the peak energy. This latter situation is similar to what is observed for the annealed sample in Fig. 1.

There is a strong correlation between the intensity of a given spectral energy region and the depth where these electrons were emitted.[56] For example, the elastic peak intensity depends strongly on the atom concentration at depths <1λ but is rather independent of the concentration at depths >3λ. On the other hand, the spectral intensity 100 eV below the peak energy depends strongly on electrons excited from atoms at 3–4λ depth but depends less on the atom concentration for depths <1λ. Different energy regions of the spectrum thus carry information on the atomic concentration at different depths. It is, however, important to note that there is a wide range of depths that contribute to the intensity at a given energy loss. This phenomenon was investigated in Ref. 56 where the wide distribution of energy loss is illustrated for model spectra from several atom depth distributions. To facilitate one's thinking while doing practical spectral analysis, it is useful to have a rough model in mind. As shown in Ref. 56, if the typical energy loss in a single scattering event is denoted by δE, then the intensity in the full energy range up to ΔE below the peak energy is primarily determined by the distribution of electron emitters within the outermost depth range, R, where

$$R = \frac{\Delta E}{\delta E}\lambda. \tag{11}$$

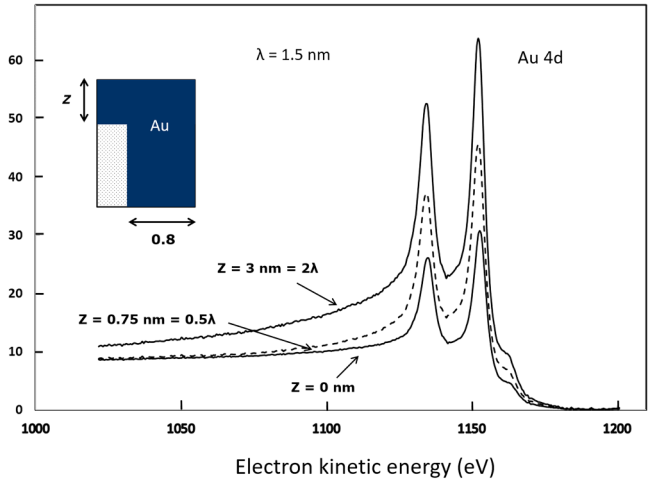

FIG. 12. Model Au4d spectra of Au without and with a surface segregation layer, which is seen to cause the peak intensity to increase. The background below the peak increases, however, only when the segregated layer has a certain thickness. QUASES (Ref. 11) was used to calculate the spectra.

δE is typically ~15–30 eV depending on the solid.[28] With ΔE = 100 eV, one gets R ~ 4–7λ. The spectrum in an energy range up to ~100 eV from the peak energy is then primarily determined by the composition within the outermost 5λ and the contribution from electrons excited at larger depths will be small. Note that Eq. (8) should never be used for anything but a very rough estimate.[56]

B. Peak area over increase in background (A_p/B) method

Another, more quantitative method to get information on the composition depth profile from the XPS peak-background was suggested many years ago.[36,60–62] It relies on the notion (see left-hand panel in Fig. 7) that the peak area and the background intensity on the low energy side change in opposite directions as the atoms are located in a layer at varying depth. Consequently, the ratio A_p/B of peak area A_p to increase in background intensity B 30 eV below the peak energy is a very sensitive parameter to the depth distribution of the atoms responsible for the peak. This is similar to the visual inspection method, but it takes into account, in a quantitative way, that it is the full peak intensity, i.e., the peak area and not the peak height that counts. It also gives a quantitative number that makes it possible to objectively compare the depth location of atoms in two samples. The value of A_p/B can also be used on an absolute scale to get insight into the depth distribution of the atoms. Thus, for a homogeneous distribution of atoms, it was found that this ratio, D_o, is almost constant (~23 eV), independent of material and peak energy. Deviations from this value can then be used to estimate the depth distribution of atoms and to estimate thin film thicknesses.[36,50,61–63]

The method is defined in Fig. 13 that shows model spectra, calculated with the QUASES software,[11] for a gold substrate with a 3 nm copper overlayer and a 1.5 nm thick gold overlayer on copper. A_p is the peak area (of the doublet in this case) determined after a linear background has been subtracted (dashed line) from the measured spectrum. The high energy for the straight line background is defined as the energy where the intensity has dropped to 10% of the intensity at the peak energy while the low energy point for the straight line is defined as the energy that is the same distance below the peak energy as the high energy point is above the peak energy.[62] B is the increase in intensity measured 30 eV below the peak energy. (In the case as here of a doublet peak, the geometrical weighted centroid of the peak structure is used as reference.) A rough estimate of the in-depth distribution of atoms can then be found from the rules in Table II. For a given system, the method may be fine-tuned by calibrating D_0 against A_p/B determined from analysis of a sample that is known to have a homogeneous atom distribution. An example of its application is also shown in Fig. 13 where the values of A_p/B for the two cases are seen to be consistent with the rules in Table II. Using the visual inspection method in Sec. V A., it is also concluded that Au in Fig. 13(a) is in the bulk, and in Fig. 13(b), gold is surface localized. The results are summarized in Table III.

Applying the method to the oxidized iron sample in Fig. 2 gives A_p/B = 3.9 and 14.8 eV for Fe2p and O1s, respectively (Table IV), and compared to Table II, this indicates that Fe is strongly subsurface while O is in a thick surface layer, slightly subsurface. On top, there is probably a thin layer of oxides corresponding to the observed Ca, Mg, and C atoms. However since the O layer is thick, there must be a thick FeOx below. The Fe distribution, being strongly subsurface, must then be interpreted as a low concentration in a large surface region, forming a thick FeOx layer, and a considerably higher Fe concentration deep in the bulk. From this, the conclusion is that the sample consists of a thick FeOx surface layer on top of pure Fe with Ca, Mg, and C oxides in the topmost layers. This is in good agreement with the more involved analysis in Sec. V D. (see Table IV), which shows that the oxide layer is ~8 nm thick and that there is a considerable overlap in the depths where both O and Fe are present.

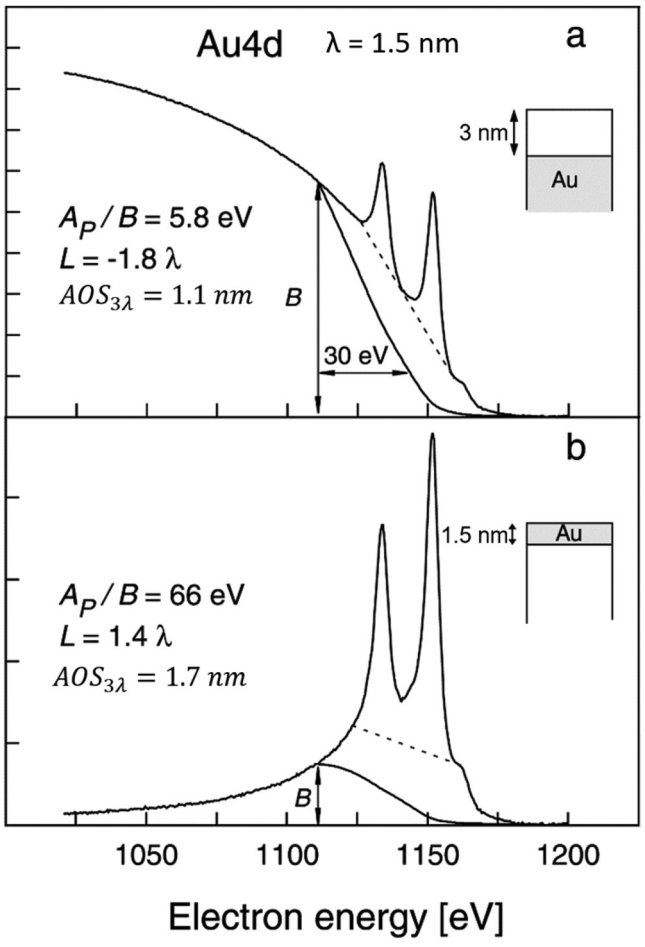

FIG. 13. Two examples of the application of the A_p/B and the decay length (L), $AOS_{3\lambda}$ methods, respectively. The two model spectra were calculated for (a) a gold substrate covered with a 3.0 nm overlayer and (b) a 1.5 nm gold film on top of a substrate. λ = 1.5 nm in both cases.

In Fig. 14, the method is applied to the Au-Ni sample in Fig. 10. For Au, A_p/B = 46 eV implies that Au is in a surface layer while A_p/B = 9.2 eV for Ni implies that Ni is in the bulk, in agreement with the results from the visual inspection method (Fig. 10).

TABLE II. Rules to estimate the atom depth distribution from A_p/B (Sec. V B).

A_p/B	Depth distribution
~23 eV	Roughly uniform
>30 eV	Surface localized
<20 eV	Subsurface localized
If the same peak from two samples has values $D_1 = \left(\frac{A_p}{B}\right)_1$ and $D_2 = \left(\frac{A_p}{B}\right)_2$, then	
If $30\text{ eV} < D_1 < D_2$	Atoms are surface localized in both samples and are at shallower depths in sample 2 than in sample 1
If $D_1 < D_2 < 20\text{ eV}$	Atoms are primarily in the bulk of both samples and at deeper depths in sample 1 than in sample 2

In Ref. 63, the A_p/B method was successfully applied to determine the growth structure of Cu_2O on Cu. Other examples of its practical application may be found in Refs 64 and 65.

A similar idea was later suggested by Salvi and Castle,[66] and a related method by Castle and Baker relies on analysis of the slope of the background signal, which clearly also varies with the depth distribution.[67,68] Another idea put forward by Seah *et al.* consists in studying the ratio of two spectra recorded at widely different emission angles,[69] which will show characteristic variations due to the difference in the effective path length for emitted electrons between the two spectra.

The main strength of the A_p/B method lies probably in its ability to easily monitor and compare the depth distribution for specific systems. It is thus very well suited for fast control of a specific system consisting of layered structures. Thus, for quality control in the production of a given thin film structure, all it takes to control the growth is to measure the total intensity in two energy windows each only a few electron volts wide: one around the peak energy and the other around 30 eV below the peak energy. Energy resolution is not essential so the spectrometer can be set at very low energy resolution, which results in high measured intensity, and very poor signal-to-noise ratios are also acceptable because it is the integrated intensity in the two energy windows that count. Therefore the required measurement to obtain A_p/B and subsequent data analysis can be done in a fraction of a second. Furthermore, since it relies on the intensity ratio at two energies that differ very little in relative energy in the spectrum, it is very robust against variations in the details of the experimental setup and is totally independent of, e.g., the photon flux. When applied to a specific system on the production line, one is not concerned with the type of growth since this is constant and has already been established for the specific system being produced, and one only needs a criterion (specified by a certain A_p/B value) to decide when to stop the deposition of layers. This method is highly effective for automated control of layer growth on the production line and is used in, e.g., the semiconductor chip industry.[54,70]

The A_p/B method was also successfully applied to obtain images of film thicknesses.[71] For imaging, one needs to acquire and analyze thousands of spectra, one for each pixel. Speed of both data acquisition and data analysis is, therefore, mandatory and are both provided by this method.

TABLE III. Results from analysis of the Au 4d spectra in Fig. 13.

Method of analysis	Au in spectrum 13 a	Au in spectrum 13 b
Visual inspection (Sec. V A)	Subsurface	Surface localized
A_p/B (Sec. V B)	5.8 eV	66 eV
Decay length L and $AOS_{3\lambda}$ (Sec. V C)	$L = -1.8\lambda$ $AOS_{3\lambda} = 1.1$ nm	$L = 1.4\ \lambda$ $AOS_{3\lambda} = 1.7$ nm
QUASES (Sec. V D)	3 nm–100 nm	0–1.5 nm

TABLE IV. Results from analysis of the O1s and Fe2p spectra in Fig. 2.

Method of analysis	Fe	O
Visual inspection (Sec. V A)	Subsurface	Thick surface layer—slightly subsurface
A_p/B (Sec. V B)	3.9 eV	14.8 eV
Decay length, L (Sec. V C)	-1.54λ	-1.95λ
QUASES (Sec. V D)	3.5–100 nm	2.5–8.0 nm

C. Decay length *L* and amount of substance $(AOS)_{3\lambda}$ method

A more advanced method was first suggested in 1990 (Refs. 20, 63, and 72) and later improved,[34] and its validity has been tested.[34,63,73–77] This method is a simplified version of the QUASES method in Sec. V D. The rationale for its development was that while QUASES analysis can give very detailed information on the atom depth distribution, it is also clear that the more details one attempts to extract from the spectra, the more careful and trained

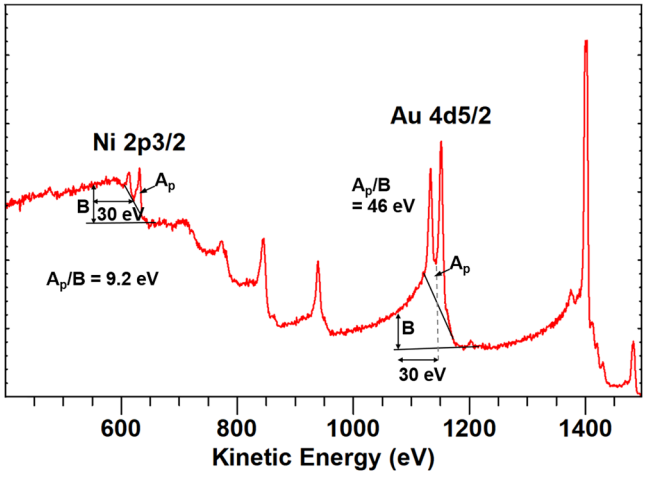

FIG. 14. Analysis of the spectrum in Fig. 10 by the Ap/B method.

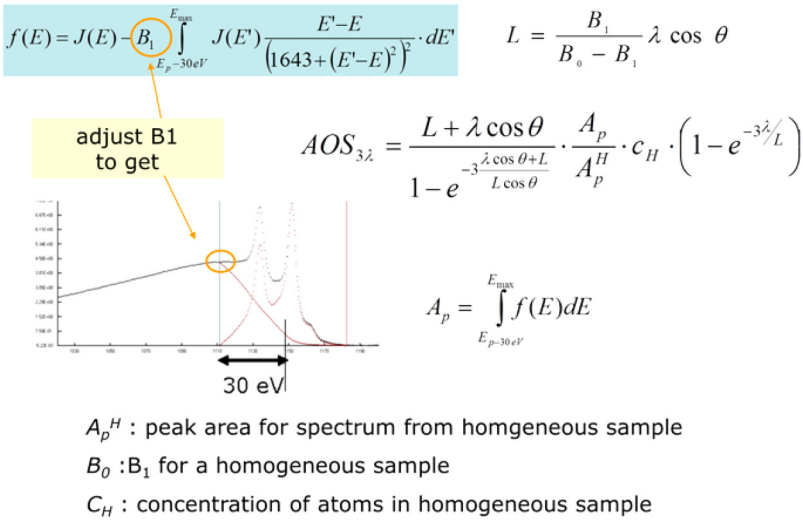

FIG. 15. Algorithm for Decay length (L), $AOS_{3\lambda}$ analysis method. The upper part shows the idea followed to create a robust method and the lower panel the resulting algorithm. Adapted with permission from Tougaard, J. Vac. Sci. Technol. A **23**, 741 (2005). Copyright 2005, American Vacuum Society.

the operator must be when preforming the analysis. Therefore rather than trying to get as much information as possible on the details of the depth distribution, in this approach, one asks for less information than what is actually available in the spectrum. This is the key to produce a very robust procedure where the result is not affected by small errors in the analysis. In this method, all depth distributions are approximated as exponential exp(-z/L), where L is a characteristic decay length for the profile (L can be positive as well as negative). The analysis determines just two numbers from the peak-background analysis: the number of atoms $(AOS)_{3\lambda}$ within the depth 3λ and their approximate depth distribution characterized by the length L.

The algorithm is illustrated in Fig. 15, which shows the simplicity of the procedure: the background is fitted by Eq. (2) to match the spectrum at a single energy point below the peak rather than over a large energy range (as with QUASES in Sec. V D). This is something you can easily ask a computer to do which makes it well suited for automation. The validity of the algorithm has been tested for both model[74] and experimental[34,73,75,76] spectra, and it has been shown to give very robust results. It was also successfully applied for 3D imaging with very noisy spectra.[76,77] $AOS_{3\lambda}$ is the amount of atoms in depths from 0 to 3λ which by this method is determined with a typical accuracy of 10%–20%,[74] and the interpretation of L in terms of the approximate depth distribution is done by the rules in Table V. It is somewhat strange that this rather simple method has not yet been incorporated in commercial software systems for routine analysis, to supplement the traditional method based on peak areas, with quantitative values for $AOS_{3\lambda}$ and L. It should, however, be noted that it is implemented in the CASAXPS software[8,75] although it is not yet integrated in the general CASAXPS quantification procedure.

Applying the method to the spectra in Fig. 13, for which $\lambda = 1.5$ nm, results in the solid line background and the values $L = -1.8\lambda$ and $+1.4\lambda$. Comparing to the rules in Table V, it is concluded that the atoms in (a) are strongly bulk localized and those in (b) are strongly surface localized, in good agreement with the actual distributions. The determined $AOS_{3\lambda}$ in Fig. 13(a) is 1.1 nm compared to the actual value $= 3\lambda - 3$ nm $= 1.5$ nm and in Fig. 13(b) $AOS_{3\lambda}$ is 1.7 nm compared to the actual value 1.5 nm (the results are summarized in Table III).

TABLE V. Rules to estimate the atom depth distribution from L (Sec. V C).

L	Depth distribution
$6\lambda < L$ or $L < -6\lambda$	Almost uniform
$-3\lambda < L < 0$	Most atoms are at depths $>1\lambda$
$0 < L < 3\lambda$	Most atoms are at depths $<1\lambda$
If the same peak from two samples has values L_1 L_2	
If $0 < L_1 < L_2 < 3\lambda$	Atoms are surface localized in both samples and are at shallower depths in sample 1 than in sample 2
If $-3\lambda < L_1 < L_2 < 0$	Atoms are primarily in the bulk of both samples and at deeper depths in sample 2 than in sample 1

Applying the method to the spectra in Fig. 2 results in decay lengths L of -1.54λ and -1.95λ for Fe and O, respectively (see Table IV). Comparing these with the rules in Table V shows that most Fe and O are at depths $>1\lambda$ and that Fe atoms are at larger depths than O. Since spectra from a reference sample and thereby A_p^H was not available, $AOS_{3\lambda}$ (see Fig. 15) cannot be evaluated.

The reader is referred to Refs. 34 and 73 for a rigorous explanation of the theoretical details and practical implementation of the algorithm. In Ref. 74, the accuracy of the method was established for different classes of depth profiles (surface layer, bulk with a surface layer, a buried layer) where in general the determined $AOS_{3\lambda}$ is typically found to be accurate to within 10%–20% and the rules in Table V for the relation between L and the depth distribution of atoms was found to be of general validity with only a few exceptions. The results were also found to be rather robust against variation in the energy distance from the peak energy where the background is matched to the spectrum (the consequence of choosing 20 or 40 eV instead of 30 eV was tested).[74]

D. More involved analysis using software

A more accurate and complete quantitative determination of the structure of a sample from XPS analysis can be obtained by performing a detailed calculation of the energy loss processes. Mainly two software are available for this: SESSA[7] and QUASES.[11]

SESSA (Refs. 6 and 7) is mainly used for quantitative XPS by analysis of peak intensities and is a powerful tool to calculate accurate peak intensities for various structures, and a recent example is published in Ref. 78. SESSA is, however, rarely used for quantitative XPS from analysis of the background although it is

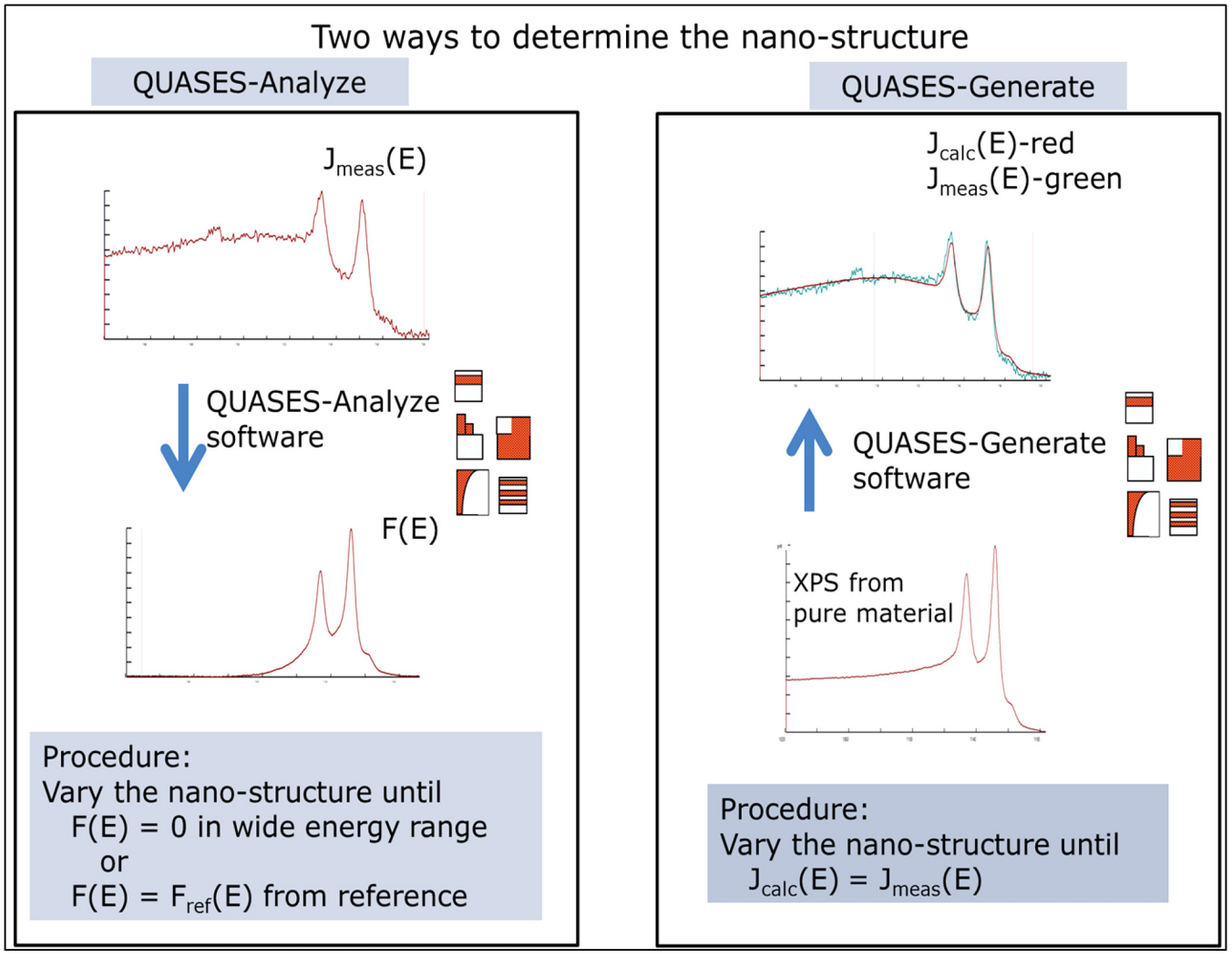

FIG. 16. Schematics showing the two different approaches for quantitative XPS analysis with QUASES software (Ref. 11).

possible, and some examples are found in Refs. 79 and 80. SESSA was also applied to study the influence of elastic scattering on the background.[48]

In contrast to this, QUASES is for quantification from analysis of both the peak intensity and the accompanying background.[10,11] The only input in QUASES is λ and the inelastic scattering cross section. The inelastic scattering cross section describes the probability for an electron to lose energy as the electron travels in the solid. It can be taken from the Universality classes[28] or from cross sections for specific materials, which are included in the software. Tailored cross sections and a mixture of cross sections can also be constructed with the software. The inelastic mean free path λ can be taken from tables,[4] the NIST database,[81] from a universal curve,[82] or it may be calculated from the TPP2M formula, e.g., by use of the free QUASES-IMFP-TPP2M software.[13]

The principle in the analysis is illustrated in Fig. 16. In QUASES, there are two ways to analyze the spectrum. With QUASES-ANALYZE, the background-corrected spectrum corresponding to an assumed structure is calculated. The model structure of the sample is varied, and the software calculates and displays the corresponding background. This is directly compared to the experimental spectrum. The correct structure is found when the calculated spectrum accounts for the measured background in a wide energy range below the peak. This determines the depth distribution of atoms. If the background-corrected spectrum is also compared on an absolute scale to the spectrum from a reference sample, then the concentration of atoms in the structure can also be determined.

With the QUASES-GENERATE software (right-hand side of Fig. 16), a model spectrum is calculated based on an input spectrum from a pure reference sample. The structure is varied until the model spectrum fits the measured spectrum on an absolute scale, and when this is achieved, the correct atom depth distribution has been determined.

This background analysis method is sensitive to depths up to $\sim 8\lambda$.[56] This is larger than the $\sim 3\lambda$ which is usually quoted for XPS[1,2] and has its origin in Eq. (1) where the exponential drops rapidly with depth. The difference is that with QUASES peak shape analysis, we probe not only the peak intensity but also the inelastically scattered electrons. Those electrons originate from larger depths (see Fig. 5), which explains why the probing depth is considerably larger.

Analysis with QUASES has become increasingly widespread over the past years. It can be applied to study a wide range of practical situations. For example, it is easy to determine whether a deposited film grows in the form of islands on a substrate.[83–85] As an example, Fig. 17 shows the spectra of Ge deposited on an Si (001) surface.[83] The best fit to the spectrum is obtained with islands of 4.5 nm height covering 45% of the surface. This was found to be in good agreement with AFM measurements of the surface topography. The uncertainty on the determined height and coverage is illustrated by the analysis in the lower panels where they have been varied by 20%. The considerably worse agreement indicates that the uncertainty on the determined height and coverage is about 5%. These are typical uncertainty values for the method. The growth structure of Cu, Ag, Au, and Pt on Si(111) were also determined by this method,[86] and it was also

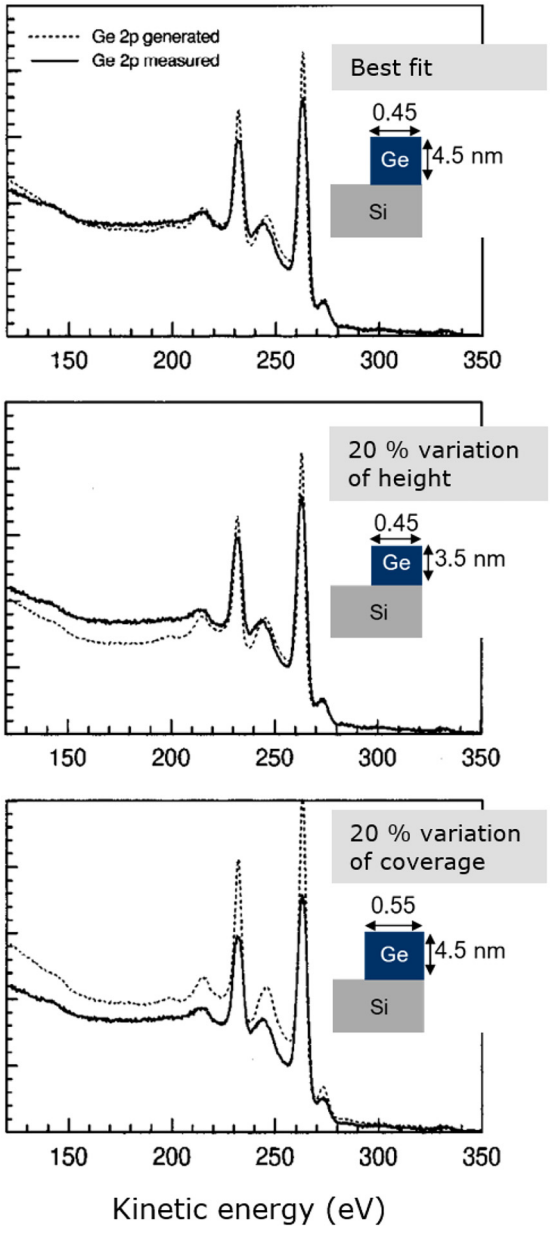

FIG. 17. Measured XPS of Ge 2p and spectra generated with QUASES. Upper panel shows the best fit achieved with a single island being 4.5 nm high and covering 45% of the surface. The lower two panels show that a considerably worse fit is obtained when the height or the coverage is changed by 20%. Data from Schleberger *et al.*, J. Vac. Sci. Technol. B **13**, 949 (1995). Copyright 1995, American Vacuum Society.

demonstrated how annealing induced diffusion of the metal atoms into the silicon can be followed nondestructively, almost as it happens in real time, by consecutively recording XPS as the temperature increases.[86] A similar application of this method to study

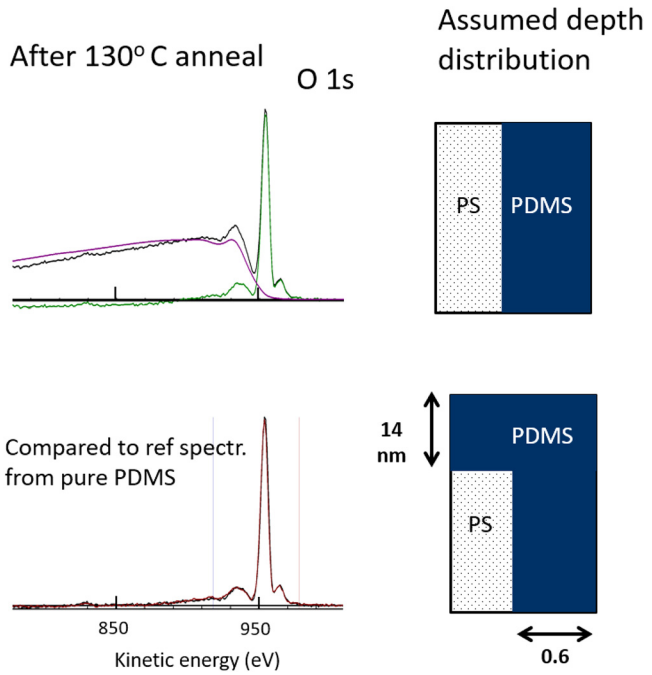

FIG. 18. QUASES analysis of the spectrum in Fig. 1 (see text).

the room temperature growth of gold nanoparticles on polystyrene (PS) and their subsequent gradual annealing induced embedding into the substrate was published in Ref. 87. There are numerous other application of the method, some of which are listed in Ref. 10.

The O1s spectrum in Fig. 1 of the diblock copolymer after annealing is analyzed in Fig. 18. The poor agreement with the background in the upper part shows that the oxygen concentration is not homogeneous in the surface region. Oxygen is a marker for PDMS, since oxygen is only in the PDMS and not in PS. The perfect agreement with a reference spectrum from pure PDMS on an absolute scale in the lower part of Fig. 18 shows that PDMS is segregated to the surface in an ~14 nm thick layer. Analysis of the Si peaks in Fig. 1 gives a similar result.

Figure 19 shows the analysis of the spectrum of the oxidized Fe sample in Fig. 2, and the conclusion is that Fe is covered by an ~3.5 nm thick overlayer while oxygen is mainly present from 2.5 to 8 nm depth (see Table IV). It is hard to analyze the Ca, Mg, and C peaks because their background ranges overlap in energy (see also Sec. V E.).

More recently, Risterucci *et al.*[88] applied QUASES to characterize the structure of deeply buried layers and interfaces in stacks using hard x-ray photoelectron spectroscopy (HAXPES). Here, the larger photon energy results in a larger inelastic mean free path for the photoelectrons and the probing depth increases [e.g., for Cu, λ increases from 0.9 nm at 0.5 keV to 5.5 nm at 5 keV (Ref. 13)]. It was previously estimated that the depth over which it is considered

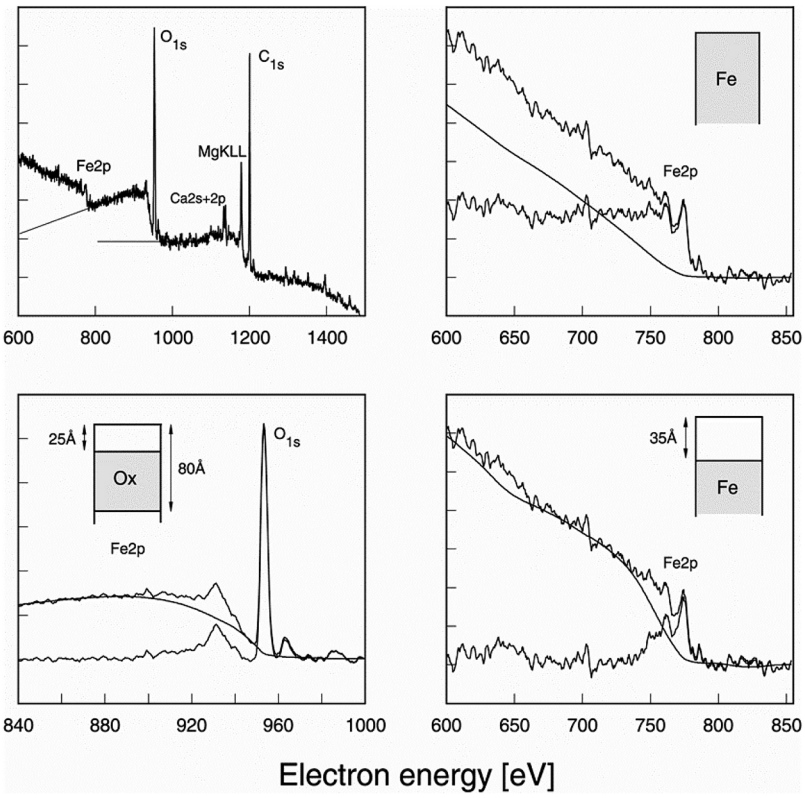

FIG. 19. QUASES analysis of the spectrum in Fig. 2 (see text).

that information can be extracted using this analysis with a standard *AlKα* source, where the inelastically scattered electrons typically can be followed over an energy range of ~100 eV, is ~8λ.[56] In HAXPES, the spectrum can often be followed over a larger range of energy loss and consequently the information depth will increase [see also Eq. (11)]. Cui *et al.*[89] found that depths up to ~20λ could be monitored in a HAXPES case where the background signal could be measured up to ~1000 eV below the peak energy. In typical cases, the probing depth with HAXPES exceeds 10λ and structures at ~50 nm, and in some cases more than 100 nm depths have been studied.[29,30,45,46,88–91]

Figure 20 shows an example[46] where an ~5 nm Ta layer is buried deeply in a stack. HAXPES was obtained with 7936 eV energy photons. The analysis in the left-hand side panel of the Ta3p3/2 peak correctly identifies the depth location of the Ta layer. Note that the peak intensity is much smaller than the background. The peaks observed in the background are caused by multiple plasmon excitations in the Al overlayer. Likewise, the analysis in the right-hand side panel identifies the distribution of Ga atoms as being present only at depth larger than ~45 nm. The gradual interdiffusion of these layers upon annealing was also determined by background analysis.[45] The wiggles observed in the background-corrected spectra are due to numerical noise caused by the almost vanishing Ta3p$_{3/2}$ and Ga2s and 2p peak intensities. This can be avoided by using reference spectra of the involved peaks from pure materials to model the spectra with QUASES-GENERATE analysis as recently demonstrated by Spencer *et al.*[91]

Elastic electron scattering can also affect both the peak intensity[6,37,38,40–43] and the shape of the background.[47,48] As discussed in Sec. II A. the effects of elastic scattering is particularly important for structures that are buried at more than 2λ depth.[38,41] The simple approximate correction for this given by Figs. 8(a) and 8(b) (Ref. 41) were applied successfully in Refs. 38, 45, and 46.

Finally, we mention two additional areas of high technological importance, namely ambient pressure XPS and core shell nanoparticles (CSNPs), where peak-background analysis was successfully applied within the past year.

Application of XPS taken under ambient pressure conditions has become widespread in recent years.[92] A problem for the interpretation of such spectra is the distortion of the spectrum caused by scattering effects as the photoelectrons travel through the gas to the spectrometer. Recently, it was shown how QUASES can be used to accurately remove this distortion and bring the spectrum back to its condition at the surface.[93]

CSNPs play a key role in many industrial applications. The properties of the CSNPs depend critically on their structure and, in particular, on the completeness of the coating, and it is important to have methods to their characterization. Recently, Müller *et al.*[94] applied QUASES analysis to study two systems that had previously been well characterized by other methods.[78] These were used as model systems to determine to what extent the detailed structure of the CSNPs could be determined with this method. Studying CSNPs with different shell thicknesses, it was shown that QUASES analysis can correctly identify not only the CSNP shell thicknesses but also deviations from ideality in terms of the heterogeneity of the shell thickness and the incomplete encapsulation of the core by the shell material.[94] For this analysis, it is necessary to prepare the CSNPs as a submonolayer dispersed on a flat substrate because otherwise there will be a significant contribution to the measured intensities from the CSNPs below. One of the model systems studied was nanoparticles with a core of PTFE [poly(tetrafluoroethylene)] coated with a shell of PS. Figure 21 shows an example analysis of the F1s spectrum from a submonolayer of PTFE-PS CSNPs spin coated on a silicon wafer. Fluorine is a marker for the presence of PTFE and is used to determine the structure of the core. The upper panel shows analysis of the F1s peak-background for a model where it is assumed that the coating is ideal. Note that the "sides"

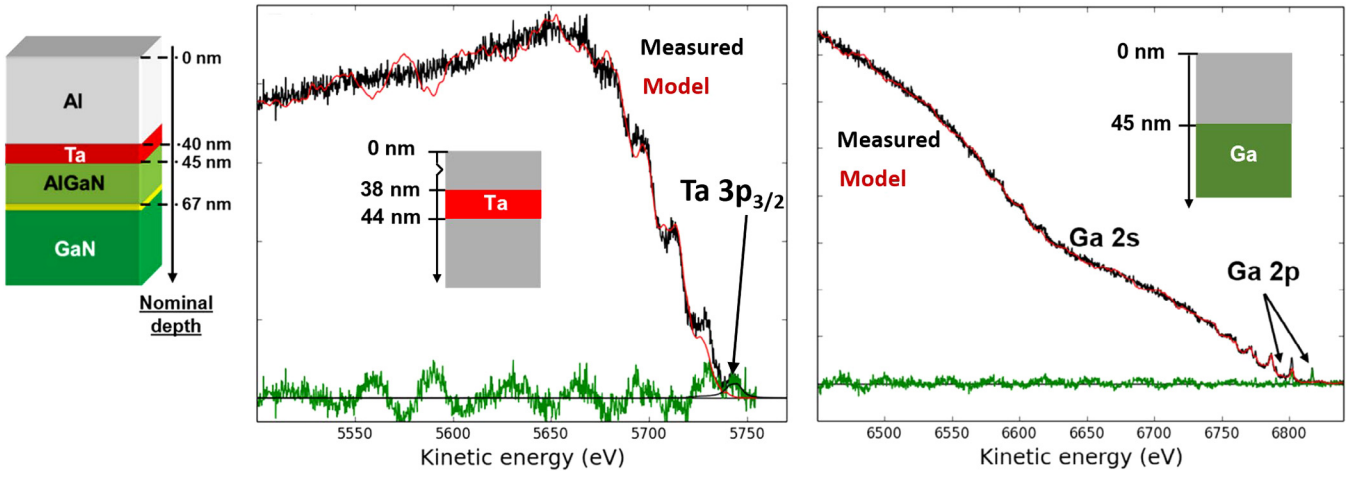

FIG. 20. HAXPES of an ~5 nm Ta layer buried ~45 nm deep in a stack excited with 7936 eV energy photons. The spectra are analyzed with QUASES-ANALYZE. Note that the Ta 3p$_{3/2}$ and Ga3p Ga3s peaks are just barely visible. Data from Zborowski *et al.*, Appl. Surf. Sci. **432**, 60 (2018). Copyright 2018, Elsevier.

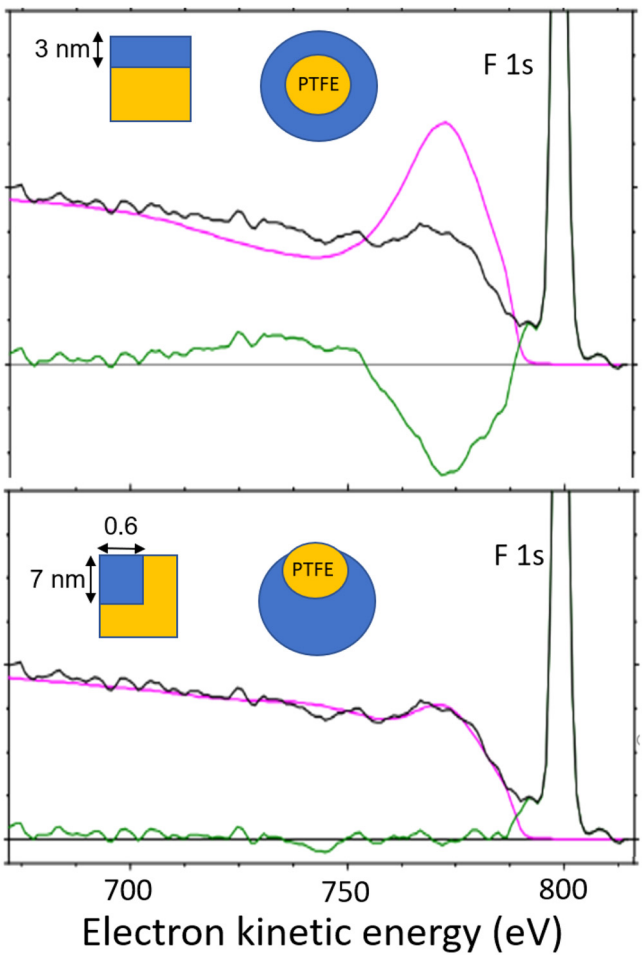

FIG. 21. QUASES analysis of a core shell nanoparticle. The poor fit of the background in the upper panel shows that the coating is not perfect while the perfect match of the background with the analysis model in the lower panel shows that the coating is incomplete. Data from Müller *et al.*, Surf. Interface Anal. **52**, 770 (2020). Copyright 2020, John Wiley and Sons Ltd.

of the coating has no influence since we analyze F1s, which is only present in the core. A layer model can, therefore, be used to represent the structure of the CSNP as shown in the inset (see Ref. 94 for details). The best overall fit of the background is obtained with a 3 nm shell thickness. The fit is good far below the peak but very bad in a region closer to the peak. The lower panel shows an analysis with a model where the heterogeneity of the coating can be varied. The excellent fit of the background in the full energy range shows that this is the correct structure and that the coating is not perfect. This is in agreement with the conclusions from TOF-SIMS measurements.[78] The CSNPs will have random orientation on the substrate, and this distribution must be taken into account when interpreting the determined structure in Fig. 21, which is an average over all orientations.

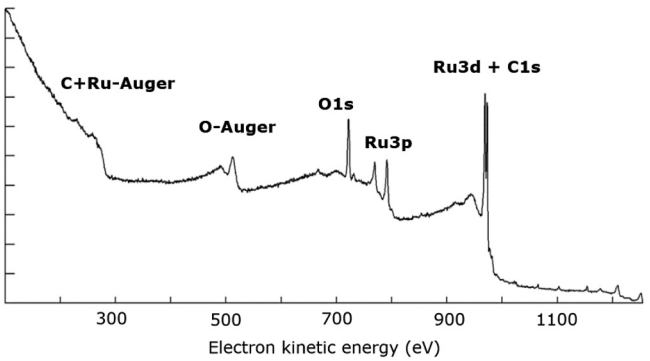

FIG. 22. XPS of a contaminated Ru film. Data from Gusenleitner *et al.*, Surf. Sci. **616**, 161 (2013). Copyright 2013, Elsevier.

E. How to select XPS peaks suitable for background analysis

The examples shown in Secs. V A–V D illustrate that analysis of the peak-background for quantitative XPS is quite easy and straightforward. This is, however, only true when, as in the examples shown, the peak-background spectral region has only contributions from atoms with the same depth distribution.

It is extremely important to apply the idea of inelastic background analysis wisely. Keep in mind that the peaks are responsible for the background. Therefore (except when using the method in QUASES-GENERATE, see below), one must make sure that the studied background range is formed exclusively from peaks that originate from one type of atoms or from several types of atoms that have the same depth distribution. So it is a necessary condition that there are no interfering peaks in an energy range of at least ~30 eV below the peak energy since even rather small peaks from other atoms in this range can obscure the results. One must also be aware of foreign peaks in a small energy range above the peak. The reason why peaks above the studied peak can cause problems is that they may add to the uncertainty on the slope of the straight line, which is subtracted to isolate the contribution to the spectrum from a single peak (see Figs. 1 and 2).

Two peaks from the same type of atom do not pose a problem, and they can be analyzed together. Note that, for example, in the analysis of the oxidized Fe sample (Fig. 19), although the Fe2p peaks involve both the metal peak and the oxidized Fe2+/3+ peaks at a few electron volts lower kinetic energy, this is not a problem because all of these peaks originate from Fe atoms (not from O atoms).

In the search for a suitable peak, it is often a minor peak that should be chosen. So when, e.g., studying Au, the Au4f or Au4d may in some situations be discarded in favor of the weaker 4p or 4s peaks. Even a very weak peak is well suited for background analysis because intensity is not so important here since the effects are so huge (Fig. 7). If an Auger peak is interfering, one can consider to use MgKα instead of AlKα as the photon source since this will shift the Auger away from the peak. Note

also that the Auger peaks can also be applied for peak-background analysis (see Fig. 23).

With HAXPES, it is usually easy to find a good peak because the higher photon energy excites deeper core levels, and the separation of these peaks is often much larger and the probability of interfering peaks is consequently smaller.

Samples involving polymers and organic films are usually easy to study by peak-background analysis. They contain besides H mainly C, O, and N, and these atoms only give rise to one sharp 1s peak and the corresponding Auger peak. So if a sample consists of a polymer and a metal, it is usually easy to find two peaks, one from the polymer and one from the metal, without interfering peaks in an energy range both below and above the peak energy.

The same is true for Si and Al, which only give rise to the 2s,2p peaks. Note also that when analyzing an SiOx film, Si2s and Si2p can be analyzed as a combined peak because they both originate from Si atoms. Likewise, the chemically shifted Si peaks due to some Si atoms bonding with oxygen is no problem because these peaks originate from Si atoms (not O atoms).

As was demonstrated by Schleberger *et al.*,[83,86] if the Si2p,2s (and similarly for Al) region has interfering peaks, one can use the Si KLL Auger peaks for peak-background analysis. These are in the energy range of 1500–1650 eV and will be sufficiently strongly excited by bremsstrahlung, when using an un-monochromatized x-ray source.

The problem with interfering peaks can, however, be a major challenge when analyzing a metal alloy composed of several

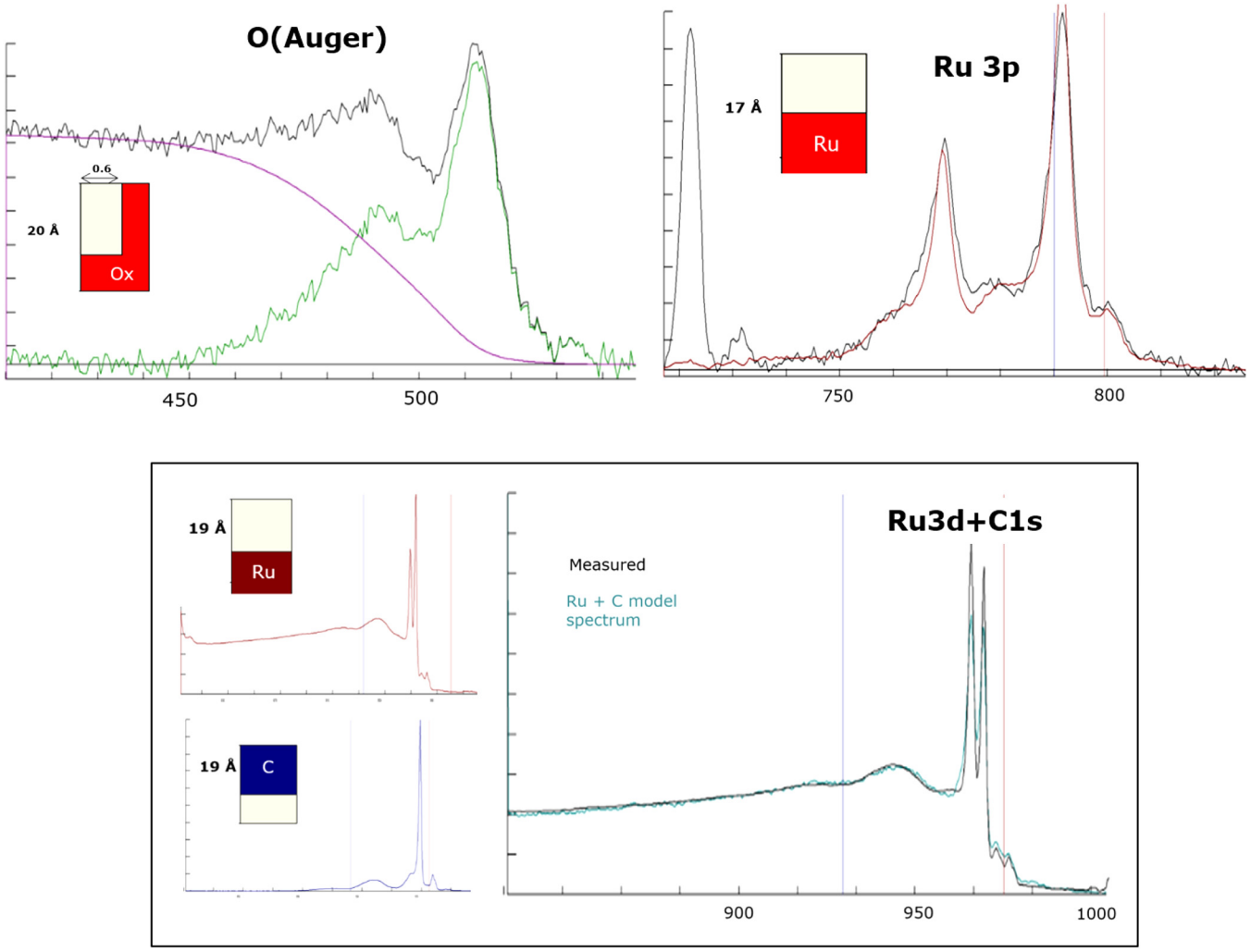

FIG. 23. Characterization of the Ru film in Fig. 22. Analysis of O (Auger), Ru3p, and the combined Ru3d and C1s peaks are shown. Data from Gusenleitner *et al.*, Surf. Sci. **616**, 161 (2013). Copyright 2013, Elsevier.

transition metals. Transition metals have typically several XPS peaks distributed over the entire survey spectrum, and if there are three or more transition metals in a sample, there will be a multitude of peaks. It can then become difficult to find a peak without interference.

In some cases, it is not possible to find a suitable peak. Then one can choose a range that involves the contribution from two (or three) different atoms and apply the QUASES-GENERATE analysis (Fig. 16) where the model spectrum is generated from spectra taken from pure materials of the involved atoms. The spectral contribution is calculated for each of the peaks, which will have different depth distributions and the sum of these generated spectra is compared with the measured spectrum. This is automatically done in the software. However, the complexity and the time spent on the analysis increase since there are more structural parameters to adjust.

Figure 22 shows a practical case studied in Ref. 95 that illustrates the considerations one should take before starting to apply background analysis. It depicts XPS of an Ru film which is used as a capping layer to protect multilayer mirrors used in high energy lithography. During use, the film gets contaminated and one wants to determine the thickness of the C and O films. From the survey spectrum, it is obvious that O Auger is very well suited for analysis. Therefore, this is done first and the analysis is straightforward and is shown in Fig. 23. This determines the oxygen depth distribution. Note that O1s is not easily analyzed because the background from the Ru peak makes it quite uncertain to judge how the straight line should be fitted to the high energy side of the O1s peak. The combined O1s and Ru3p energy range could, however, be analyzed with QUASES-GENERATE. Next, one observes that the Ru3p peak does have an interfering O1s peak with the MgKα satellite 55 eV below the centroid of the Ru 3p peak (using a monochromatized source would allow to use a 10 eV wider energy range). So analysis of Ru is possible in this limited energy range, which determines the depth distribution of Ru as shown in Fig. 23. It is however impossible to isolate the contribution to the spectrum from C atoms because there is an almost exact coincidence in the C1s and Ru3d peak energies and the same is true for C Auger, which overlaps with the Ru Auger peaks. Carbon can, therefore, only be analyzed by generating spectra from Ru and C and adding these to be compared with the measured spectrum. In QUASES-GENERATE, there are facilities to do this interactively, and the result is shown in the lower part of Fig. 23. In modeling, the knowledge on the Ru atom distribution can be used to facilitate the fitting procedure.

VI. SUMMARY

In this guide, we first discuss the problem with standard quantitative XPS analysis which, based on measured peak intensities, calculates and reports the composition as atomic concentrations of the surface. We point out that these numbers can be highly misleading and very inaccurate and that a meaningful quantification cannot be made unless the attenuation factor is also taken into account. In Secs. IV A–IV C, we then discuss the advantages and limitations of different ways to do that. We emphasize the interplay between XPS peak intensity, inelastic background, and depth distribution of atoms and describe how this can be used to significantly improve the accuracy and greatly enhance the amount of information that can be extracted from XPS. The quantification then involves the analysis of both the peak intensity as well as the distribution of inelastically scattered electrons in the background that accompanies the peak. This has resulted in several practical methods and algorithms that involve spectral analysis at different levels of complexity as described in Secs. V A–V D. Finally, Sec. V E gives details on how the best peaks are selected for analysis by these methods.

DATA AVAILABILITY

The data that support the findings of this study are available from the corresponding author upon reasonable request.

REFERENCES

[1]D. Briggs and J. T. Grant, *Surface Analysis by Auger and X-Ray Photoelectron Spectroscopy* (IM-Publications, Manchester, 2003), ISBN 1 901019047.
[2]J. F. Watts and J. Wolstenholme, *An Introduction to Surface Analysis by XPS and AES* (Wiley, Chichester, 2003).
[3]C. J. Powell, Microsc. Today **24**, 16 (2016).
[4]S. Tanuma, C. J. Powell, and D. R. Penn, Surf. Interface Anal. **43**, 689 (2011).
[5]M. Mohai, Surf. Interface Anal. **36**, 828 (2004).
[6]W. Smekal, Wolfgang S. M. Werner, and Cedric J. Powell, Surf. Interface Anal. **37**, 1059 (2005).
[7]W. S. M. Werner and C. J. Powell, *NIST Database for the Simulation of Electron Spectra for Surface Analysis (SESSA): SRD 100 Version 2.1* (NIST, Gaithersburg, MD, 2018), see https://catalog.data.gov/dataset/nist-simulation-of-electron-spectraforsurface-analysis-sessa-srd-100.
[8]N. Fairley, *CasaXPS: Processing Software for XPS, AES, SIMS and More* (Casa Software Ltd., Teignmouth, 2018), see http://www.casaxps.com/.
[9]R. Hesse, *Unifit for Windows: The Art of the Peak fit: Spectrum Processing, Peak Fitting, Analysis and Presentation Software for XPS, AES, XAS and RAMAN Spectroscopy Based on WINDOWS* (Unifit Scientific Software GmbH, Leipzig, 2020), see http://www.unifit-software.de/.
[10]S. Tougaard, J. Electron Spectrosc. Relat. Phenom. **178**, 128 (2010).
[11]S. Tougaard, *Software Packages to Characterize Surface Nano-Structures by Analysis of Electron Spectra* (QUASES.com, Odense, 2020), see http://www.quases.com/products/quases-tougaard/.
[12]T. S. Lassen and S. Tougaard, *Software Packages to Characterize Surface Nano-Structures by Analysis of Electron Spectra* (QUASES.com, Odense, 2020), see http://www.quases.com/products/quases-arxps/.
[13]S. Tougaard, *QUASES-IMFP-TPP2M Ver.4.1* (QUASES.com, Odense, 2020), see http://www.quases.com/products/quases-imfp-tpp2m/.
[14]D. Shah, D. I. Patel, T. Roychowdhury, B. G. Rayner, N. O'Toole, D. R. Baer, and M. R. Linford, J. Vac. Sci. Technol. B **36**, 062902 (2018).
[15]D. R. Baer *et al.*, J. Vac. Sci. Technol. A **37**, 031401 (2019).
[16]C. R. Brundle and B. V. Crist, J. Vac. Sci. Technol. A **38**, 041001 (2020).
[17]A. G. Shard, J. Vac. Sci. Technol. A **38**, 041201 (2020).
[18]C. D. Easton, C. Kinnear, S. L. McArthur, and T. R. Gengenbach, J. Vac. Sci. Technol. A **38**, 023207 (2020).
[19]M. H. Engelhard, D. A. Baer, A. Herrera-Gomez, and P. Sherwood, J. Vac. Sci. Technol. A **38**, 063203 (2020).
[20]S. Tougaard, J. Vac. Sci. Technol. A **8**, 2197 (1990).
[21]S. Tougaard, J. Vac. Sci. Technol. A **14**, 1415 (1996).
[22]M. P. Seah, J. Electron Spectrosc. Relat. Phenom. **71**, 191 (1995).
[23]T. H. Andersen, S. Tougaard, N. B. Larsen, K. Amdal, and I. Johannsen, J. Electron Spectrosc. **121**, 93 (2001).
[24]S. Tougaard, "Quantification of surface and near-surface composition by AES and XPS," in *Handbook of Surface and Interface Analysis: Methods for*

Problem-Solving, 2nd ed., edited by J. C. Rivière and S. Myhra (Taylor and Francis, New York, 2009), pp. 223–245, ISBN 13: 978-0-8493-7558-3.
[25]D. A. Shirley, Phys. Rev. B **5**, 4709 (1972).
[26]S. Tougaard, Surf. Sci. **216**, 343 (1989).
[27]C. Jansson *et al.*, Surf. Interface Anal. **23**, 484 (1995).
[28]S. Tougaard, Surf. Interface Anal. **25**, 137 (1997).
[29]P. Risterucci, O. Renault, C. Zborowski, D. Bertranda, A. Torresa, J.-P. Rueffc, D. Ceolin, G. Grenet, and S. Tougaard, Appl. Surf. Sci. **402**, 78 (2017).
[30]C. Zborowski and S. Tougaard, Surf. Interface Anal. **51**, 857 (2019).
[31]S. Tougaard, Phys. Rev. B **34**, 6779 (1986).
[32]S. Tougaard, Surf. Interface Anal. **11**, 453 (1988).
[33]S. Tougaard and H. S. Hansen, Surf. Interface Anal. **14**, 730 (1989).
[34]S. Tougaard, J. Vac. Sci. Technol. A **23**, 741 (2005).
[35]M. P. Seah, J. Electron Spectrosc. Relat. Phenom. **100**, 55 (1999).
[36]S. Tougaard, Surf. Interf. Anal. **8**, 257 (1986).
[37]S. Tougaard og and P. Sigmund, Phys. Rev. B **25**, 4452 (1982).
[38]S. Tougaard and A. Jablonski, Surf. Interface Anal. **25**, 404 (1997).
[39]A. Jablonski and S. Tougaard, Surf. Interface Anal. **26**, 17 (1998).
[40]A. Jablonski and S. Tougaard, Surf. Sci. **432**, 211 (1999).
[41]A. Jablonski and S. Tougaard, Surf. Interface Anal. **26**, 374 (1998).
[42]W. S. M. Werner, Surf. Interface Anal. **31**, 141 (2001).
[43]A. Jablonski and C. J. Powell, Surf. Sci. **606**, 644 (2012).
[44]S. Tougaard and A. Jablonski, Surf. Interface Anal. **23**, 559 (1995).
[45]C. Zborowski, O. Renault, A. Torres, C. Guedj, Y. Yamashita, S. Ueda, G. Grenet, and S. Tougaard, J. Appl. Phys. **124**, 085115 (2018).
[46]C. Zborowski, O. Renault, A. Torres, Y. Yamashita, G. Grenet, and S. Tougaard, Appl. Surf. Sci. **432**, 60 (2018).
[47]I. S. Tilinin, A. Jablonski, and S. Tougaard, Phys. Rev. B **52**, 5935 (1995).
[48]C. J. Powell, S. Tougaard, W. S. M. Werner, and W. Smekal, J. Vac. Sci. Technol. A **31**, 021402 (2013).
[49]S. Tougaard, Surf. Interface Anal. **50**, 657 (2018).
[50]H. Iwai, J. S. Hammond, and S. Tanuma, J. Surf. Anal. **15**, 264 (2009).
[51]P. J. Cumpson, J. Electron Spectrosc. Relat. Phenom. **73**, 25 (1995).
[52]S. Oswald and F. Oswald, Surf. Interface Anal. **40**, 700 (2008).
[53]K. Artyushkova, J. Electron Spectrosc. Relat. Phenom. **178–179**, 292 (2010).
[54]C. R. Brundle, G. Contia, and P. Mack, J. Electron Spectrosc. Relat. Phenom. **178–179**, 433 (2010).
[55]A. I. Martin-Concepción, F. Yubero, J. P. Espinos, J. Garcia, and S. Tougaard, Surf. Interface Anal. **36**, 788 (2004).
[56]S. Tougaard, Surf. Interface Anal. **26**, 249 (1998).
[57]S. Tougaard, J. Surf. Anal. **24**, 107 (2017).
[58]A. G. Shard and S. J. Spencer, Surf. Interface Anal. **49**, 1256 (2017).
[59]A. C. Simonsen, J. P. Pohler, C. Jeynes, and S. Tougaard, Surf. Interface Anal. **27**, 52 (1999).
[60]S. Tougaard og and A. Ignatiev, Surf. Sci. **129**, 355 (1983).
[61]S. Tougaard, Surf. Sci. **162**, 875 (1985).
[62]S. Tougaard, J. Vac. Sci. Technol. A **5**, 1275 (1987).
[63]S. Tougaard, W. Hetterich, A. H. Nielsen, and H. S. Hansen, Vacuum **41**, 1583 (1990).
[64]L.-S. Johansson, J. Campbell, K. Koljonen, M. Kleen, and J. Buchert, Surf. Interface Anal. **36**, 706 (2004).
[65]K. Idla, L.-S. Johansson, J. M. Campbell, and O. Inganäs, Surf. Interface Anal. **30**, 557 (2000).
[66]A. M. Salvi and J. E. Castle, J. Electron Spectrosc. Relat. Phenom. **94**, 73 (1998).
[67]J. E. Castle and M. A. Baker, J. Electron Spectrosc. Relat. Phenom. **105**, 245 (1999).
[68]J. E. Castle, J. Vac. Sci. Technol. A **25**, 1 (2007).
[69]M. P. Seah, J. H. Qiu, P. J. Cumpson, and J. E. Castle, Surf. Interface Anal. **21**, 336 (1994).
[70]C. R. Brundle, Surf. Interface Anal. **42**, 770 (2010).
[71]J. Walton and N. Fairley, J. Electron Spectrosc. Relat. Phenom. **148**, 29 (2005).
[72]S. Tougaard, H. S. Hansen, and M. Neumann, Surf. Sci. **244**, 125 (1991).
[73]S. Tougaard, J. Vac. Sci. Technol. A **21**, 1081 (2003).
[74]S. Tougaard, J. Vac. Sci. Technol. A **31**, 031503 (2013).
[75]J. Walton, M. R. Alexander, N. Fairley, P. Roach, and A. G. Shard, Surf. Interface Anal. **48**, 164 (2016).
[76]S. Hajati, S. Coultas, C. Blomfield, and S. Tougaard, Surf. Interface Anal. **40**, 688 (2008).
[77]Shaaker Hajati, Sven Tougaard, John Walton, and Neal Fairley, Surf. Sci. **602**, 3064 (2008).
[78]A. Müller *et al.*, J. Phys. Chem. C **123**, 29765 (2019).
[79]N. S. Faradzhev, S. B. Hill, and C. J. Powell, Surf. Interface Anal. **49**, 1214 (2017).
[80]G. Olivieri, K. M. Parry, R. D'Auria, D. J. Tobias, and M. A. Brown, J. Phys. Chem. B **122**, 910 (2018).
[81]NIST Electron Inelastic Mean Free Path Database Ver 1.2., see https://www.nist.gov/srd/nist-Standard-Reference-Database-71.
[82]M. P. Seah, Surf. Interface Anal. **44**, 497 (2012).
[83]M. Schleberger, A. C. Simonsen, S. Tougaard, J. L. Hansen, and A. Nylandsted Larsen, J. Vac. Sci. Technol. A **15**, 3032 (1997).
[84]D. Díaz-Fernández *et al.*, Surf. Sci. **624**, 145 (2014).
[85]L. Cattin, S. Tougaard, N. Stephant, S. Morsli, and J. C. Bernède, Gold Bull. **44**, 199 (2011).
[86]M. Schleberger, D. Fujita, C. Scharfschwerdt, and S. Tougaard, J. Vac. Sci. Technol. B **13**, 949 (1995).
[87]S. Hajati, V. Zaporojtchenko, F. Faupel, and S. Tougaard, Surf. Sci. **601**, 3261 (2007).
[88]P. Risterucci, O. Renault, E. Martinez, B. Detlefs, V. Delaye, J. Zegenhagen, C. Gaumer, G. Grenet, and S. Tougaard, Appl. Phys. Lett. **104**, 051608 (2014).
[89]Y. Cui *et al.*, J. Appl. Phys. **121**, 225307 (2017).
[90]O. Renault, C. Zborowski, P. Risterucci, C. Wiemann, G. Grenet, C. M. Schneider, and S. Tougaard, Appl. Phys. Lett. **109**, 011602 (2016).
[91]B. F. Spencer *et al.*, "Inelastic background modelling applied to Hard X-ray Photoelectron Spectroscopy of deeply buried layers: a comparison of synchrotron and lab-based (9.25 keV) measurements," Appl. Surf. Sci. (in press).
[92]Chris Arble, Meng Jia, and John T. Newberg, Surf. Sci. Rep. **73**, 37 (2018).
[93]S. Tougaard and M. Greiner, Appl. Surf. Sci. **530**, 147243 (2020).
[94]A. Müller, K. Sparnacci, W. E. S. Unger, and S. Tougaard, Surf. Interface Anal. **52**, 770 (2020).
[95]S. Gusenleitner, D. Hauschild, T. Graber, D. Ehm, S. Tougaard, and F. Reinert, Surf. Sci. **616**, 161 (2013).